Modelling and Control of Two-Phase Phenomena: Liquid-Liquid Two-Phase Flow Systems

Neima Brauner

School of Engineering,
Tel-Aviv University
Tel-Aviv 69978, Israel

1 General Description of Liquid-Liquid Flows: Flow Patterns

Flows of two immiscible liquids are encountered in a diverse range of processes and equipments. In particular in the petroleum industry, where mixtures of oil and water are transported in pipes over long distances. Accurate prediction of oil-water flow characteristics, such as flow pattern, water holdup and pressure gradient is important in many engineering applications. However, despite of their importance, liquid-liquid flows have not been explored to the same extent as gas-liquid flows. In fact, gas-liquid systems represent a very particular extreme of two-fluid systems characterized by low-density ratio and low viscosity ratio. In liquid-liquid systems the density difference between the phases is relatively low. However, the viscosity ratio encountered extends over a range of many orders of magnitude. Table 1.1 summarizes experimental studies reported in the literature on horizontal oil-water pipe flows, while studies on inclined and vertical systems are summarized in Table 1.2 and 1.3. (The tables can be found at the end of the end of this article after the bibliography). These tables reflect the wide range of physical properties encountered. Moreover, oils and oil-water emulsions may show a Newtonian or non-Newtonian rheological behavior. Therefore, the various concepts and results related to gas-liquid two-phase flows cannot be readily applied to liquid-liquid systems.

Diverse flow patterns were observed in liquid-liquid systems. In most of the reported studies the identification of the flow pattern is based on visual observations, photographic/video techniques, or on abrupt changes in the average system pressure drop. In some recent studies, the visual observation and pressure drop measurements are backed-up by conductivity measurements, high frequency impedance probes or Gamma densitometers for local holdup sampling, or local pressure fluctuations and average holdup measurements (see Tables 1.1 to 1.3). The flow patterns can be classified into four basic prototypes: Stratified layers with either smooth or wavy interface; Large slugs, elongated or spherical, of one liquid in the other; A dispersion of relatively fine drops of one liquid in the other; Annular flow, where one of the liquids forms the core and the other liquid flows in the annulus. In many cases, however, the flow pattern consists of a combination of these basic prototypes.

Sketches of various possible flow patterns observed in horizontal systems are given in Figure 1.1. Stratified flow with a complete separation of the liquids may prevail for some limited range of relatively low flow rates where the stabilizing gravity force due to a finite density difference is dominant (Figure 1.1a). It is possible that one of the layers is discontinuous, and the flow structure is stratified layers of a free liquid and a dispersion of the

other liquid (Figure 1.1c-d). With increasing the flow rates, the interface displays a wavy character with possible entrainment of drops at one side or both sides of the interface (Figure 1.1b, 1.1e-g). The entrainment process increases with increasing the flow rates. When the lighter and heavier phases are still continuous at the top and bottom of the pipe, but there is a concentrated layer of drops at the interface, a three layer structure is formed (Figure 1.1h). Eventually, for sufficiently high water flow rate, the entire oil phase becomes discontinuous in a continuous water phase resulting in an oil-in-water dispersion or emulsion (Figure 1.1i). An emulsion is a stable dispersion. Vice versa, for sufficiently high oil flow rate, the water phase may be completely dispersed in oil phase resulting in a water-in-oil dispersion or emulsion (Figure 1.1j). It is also possible for oil-in-water and water-in-oil dispersions to coexist. Impurities and high mixture velocities may yield a foam like structure of intensively intermixed oil and water, possibly with occasional appearance of clusters of one of the liquids. There are operating conditions under which

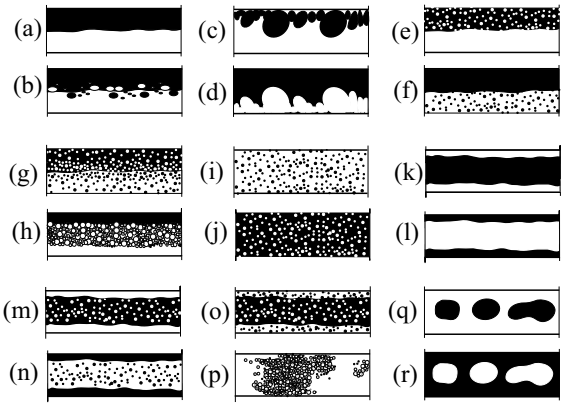

Figure 1 **a/b** Stratified flow of two separated layers (S, possibly with mixing at the interface, SM). **c/d** Stratified layers of a free-liquid and a dispersion of the other liquid (e.g. oil-in-water dispersion above a water layer, Do/w&w). **e/f** Stratified layers of a free liquid and a dispersion in the other liquid (e.g. oil and oil-in-water dispersion, Do/w&o; water and water-in-oil dispersion, Dw/o&w). **g/h** Layers of dispersions (e.g. water-in-oil dispersion above oil in water dispersion Dw/o&o/w, possibly with pure oil at the top and/or water at the bottom). **i/j** Fully dispersion or emulsion of one liquid in the other liquid (e.g. water-in-oil or oil-in-water dispersion or emulsion, Dw/o or Do/w). **k/l** Core-annular flow – a core of one liquid within the other liquid (e.g. a core of viscous oil and water in the annulus, ANw. Oil in the annulus, ANo). **m/n** Annular flow of a liquid with a dispersion in the core (water in the annulus DANw, oil in the annulus DANo). **o** Core-annular flow of two dispersions (CADw or CADo). **p** Intermittent flow (one liquid alternately occupying the pipe as a free liquid or as a dispersion, Io or Iw). **q/r** Large elongated or spherical bubbles of one liquid in the other (SLo,Bo or SLw,Bw).

an oil-in-water dispersion will change to water-in-oil dispersion. This phenomena is referred in the literature as phase inversion and is associated with an abrupt change in the frictional pressure drop (see Figure 15 in Brauner, 1998). [1]

Under certain conditions, the oil and water may stabilize in annular-core configuration (Figures 1.1k-ℓ). The flow of a viscous oil in a core, which is lubricated by a water film in the annulus (core flow), is most attractive from the viewpoint of pressure drop reduction in transportation of highly viscous oils. With increasing the water rate, the viscous core breaks up to either large slugs and bubbles, (Figure 1.1q) or into oil dispersion flowing in a continuous water phase (Figure 1.1i or q). It is possible to have also "inverted" annular flow with the oil flowing in the annulus (Figures 1.1ℓ or n). Comparison of experimental flow pattern maps reported in the literature for horizontal oil-water systems of relatively low viscosity ratio, $\mu_o/\mu_w < 100$ and $\Delta\rho/\rho_w \geq 0.1$ (shown in Brauner, 1998, Figure 2) indicated a general similarity between the sequence of the observed flow patterns and the stratified flow boundaries, but differences in the classification of the various dispersed flow regimes and the associated transitional boundaries. However, some of the reported transitional boundaries actually represent gradual changes in the dispersions structure

[1] A copy of this reference can be downloaded from http://www.eng.tau.ac.il/~brauner/LL-Flow

and the associated pressure drop, and are therefore susceptible to subjective judgment and variations. When the water is the continuous phase, oil viscosity seems to have a minor effect on the flow patterns. However, the oil viscosity affects the location of the phase inversion from Dw/o to Do/w. The input water-cut, $U_{\rm ws}/U_m$ required to invert the dispersion decreases with increasing the oil viscosity. Core flow (water annulus) is usually not obtained in oil-water systems of relatively low oil viscosity and relatively high $\Delta\rho$.

As in gas-liquid systems, the flow pattern depends on the liquids flow rates and physical properties, tube diameter and inclination. However, due to the relatively low density differential between the two-fluids, the role of gravity in liquid-liquid systems diminishes. Therefore, wall-wetting properties of the liquids and surface tension forces become important and may have a significant effect on the flow pattern. For instance, in stratified flow the interface between the liquid phase is not necessarily planar. The common assumption of a plane interface (Fig. 1.2a) is appropriate for horizontal gas-liquid systems, which are dominated by gravity. In fact, systems of low density differential as oil-water systems, resemble reduced gravity systems and capillary systems, where surface forces become important. The wetting liquid tends to climb over the tube wall resulting in a curved (concave or convex) interface (Fig. 1.2b or h). Stratified flows with curved interfaces in liquid-liquid systems have been obtained both experimentally (Valle and Kvandel, 1995, Angeli et al., 2002, Gat, 2002) and in numerical simulations (Ong et al., 1994). The possible stratified flow configurations extend from fully eccentric core of the upper phase (Fig. 1.2c) to fully eccentric core of the lower phase (Fig. 1.2g). Hydrodynamic forces may also cause the core phase to detach from the wall surface to form an eccentric core-annular configuration. However, due to a density differential between the core phase and the annular phase, the core usually stabilizes in an eccentric position (Fig. 1.2d or f) rather than in a concentric position (Fig. 1.2c). Break-up of the top (or bottom) wall film due to the float-up tendency of light (or heavier) core phase results in stratification of the fluids.

The occurrence of annular flow in liquid-liquid systems is therefore more frequently encountered in oil-water systems of low density differential, $\Delta\rho$ and small diameter tubes. These systems are characterized by a small non-dimensional Eotvös number, $Eo_D = \frac{\Delta\rho g D^2}{8\sigma} \ll 1$ and resemble micro-gravity systems. In such systems, an annulus of the wetting phase (surrounding a core of the non-wetting phase) is a natural configuration which complies with surface tension forces and wall-adhesion forces. However, for specified operational conditions, different flow patterns may result by changing the tube material (hydrophobic or hydrophilic). The start-up procedure (oil flowing in the pipe and then introducing water or vice versa), which affects the effective liquids-wall adhesion, or entry conditions (type of nozzle used to introduce the two-liquids) are also important factors in controlling the flow pattern.

In vertical upward flow and low oil viscosities, the observed flow patterns typically include oil drops, bubbles or slugs in water, transitional flow (TF, churn), water drops in oil and oil-in-water or water-in-oil emulsions (see Figure 5.3, Section 5). The physical interpretation of flow patterns transitions is similar to that described for vertical gas-liquid systems. However, the clearly defined bullet-shaped bubbles that characterize slug flow in gas-liquid slug flow are normally not observed in oil-water systems. The churn flow

is characterized as intermittent flow of complex and irregular structures of continuous oil phase (oil-dominated) and continuous water phase (water-dominated). The drops size decreases with increasing the mixture velocity, and for high velocity the liquids, either homogeneous Dw/o or Do/w of fine droplets are formed.

The organized flow pattern data on inclined liquid-liquid systems in the literature is rather limited (see Table 1.2). In large Eo_D systems, a considerable drift between the lighter oil phase and water phase exists at low mixture velocities. Under such conditions, even a moderate inclination from the vertical affects intermittency in the flow with regions of back-flow of the heavier phase (Vigneau et al., 1988 and Flores et al., 1997, Figure 7 shown in Brauner, 1998). It is to be noted that the stratified pattern typically vanishes for steeper upward inclinations than $\approx 30^o$, compared to gas-liquid systems where the stratified flow vanishes already for shallow upward inclinations.

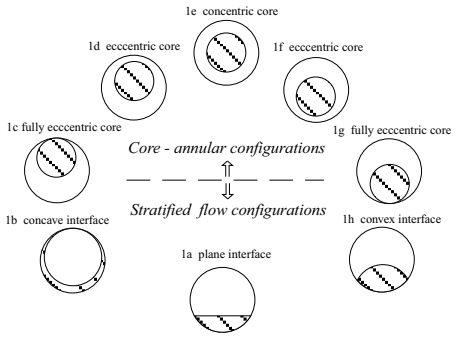

Figure 1.2 Schematic description of various configurations of separated flows.

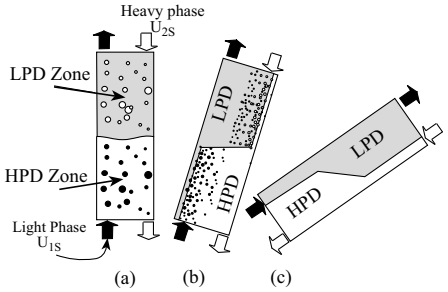

Figure 1.3 Flow patterns in countercurrent flow, a. vertical, b. off-vertical, c. inclined column.

Counter-current liquid-liquid flow is frequently encountered in the process industry. Figure 3 shows a schematic description of the flow patterns obtained in a column in counter-current flow of relatively low flow rates (Ullmann, et al., 2001). In a vertical column (Figure 3a), the basic flow pattern is dispersed flow, with either the heavy phase dispersed in the light phase (light phase dominated, LPD), or the light phase dispersed in the heavy phase (heavy phase dominated, HPD). These two configurations of dispersed flow can be simultaneously obtained in the column, separated by an interface. The latter can be placed at any position along the column by manipulating the resistance at the heavy phase outlet. With a sufficiently low (high) resistance, the flow pattern in the entire column is LPD (HPD), respectively. In systems of $Eo_D \gg 1$, the phases tend to segregate with a slight off-vertical positioning of the column (Figure 3b). The two configurations obtained in this case correspond to stratified-dispersed flow both in the HPD (Do/w&o) and in the LPD (Dw/o&w) zones. Further inclining the tube results in a complete segregation of the phases. In an inclined tube (Figure 3c), the basic flow pattern in both zones is stratified flow with either a wavy or smooth interface. The flow in the HPD (LPD) zone corresponds to a thick (thin) layer of the heavy phase flowing

counter-currently to a thin (thick) layer of the light phase. Similarly to the operation of a vertical column, the location of the interface between these two zones can be controlled by adjusting the resistance at the heavy phase outlet. Thereby, the entire column can be occupied by either one of these two flow configurations, or by both of them.

The various flow patterns are associated with different pressure drop, in situ holdup, heat transfer coefficient and other related phenomena, such as fouling and corrosion of the pipe. Therefore, generalized models which attempt to cover the whole range of different liquid properties and different flow patterns (e.g. Charles and Lillelcht, 1966, Theissing, 1980) can only be approximate. The accepted approach today consists of predicting the flow pattern under specified operational conditions (see Section 5) and applying an appropriate model (see Sections 2,3,4).

2 Stratified Flow

Stratified flow is considered a basic flow pattern in horizontal or slightly inclined liquid-liquid systems of a finite density differential, since for some range of sufficiently low flow rates, the two liquids phases tend to segregate. The modeling of liquid-liquid stratified flows requires the consideration of additional aspects in comparison to gas-liquid stratified flows. Due to the variety of physical properties that may be encountered, it is not a priori evident which of the phases is the faster (for specified operational conditions). Therefore, the ambiguity concerning the appropriate closure law for representing the interfacial shear is even greater than in the case of gas-liquid flows. Multiple solutions can be obtained for specified operation conditions in co-current and counter-current inclined flows, which are relevant in practical applications. Moreover, as a result of the relatively low density difference, surface tension and wetting effects become important, and the interface shape (convex, concave, plane) is an additional field that has to be solved.

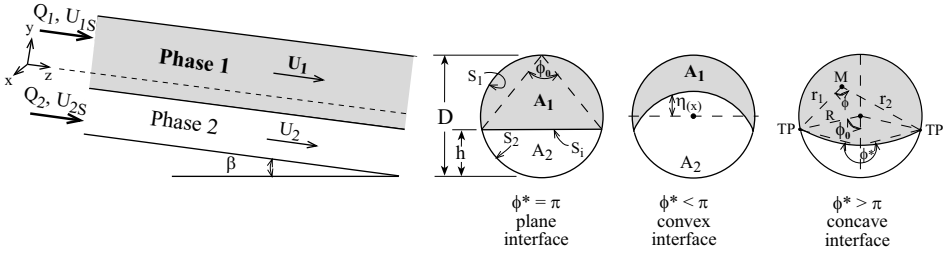

Figure 2.1 Schematic description of stratified flow configuration and parameters.

The stratified flow configuration and coordinates are illustrated in Figure 2.1. A configuration of a curved interface is associated with a different location of the triple point (TP) and thus, with a variation in the contact area between the two fluids and between the fluids and the pipe wall. Depending on the physical system involved, these variations can have prominent effects on the pressure drop and transport phenomena. On the other hand, the feasibility of obtaining exact solutions for stratified flows is restricted to laminar-laminar flows, which are of limited relevance to practical applications of gas-liquid two phase flows. However, laminar flow in both phases is frequently encountered in liquid-liquid systems.

Given the location of the fluids interface, the 2-D velocity profiles in steady and fully developed axial laminar flow of stratified layers, $u_1(x,y), u_2(x,y)$ are obtained via analytical or numerical solutions of the following Stokes equations (in the z direction, see Figure 2.1):

$$\mu_1 \left(\frac{\partial^2 u_1}{\partial x^2} + \frac{\partial^2 u_1}{\partial y^2} \right) = \frac{\partial P_1}{\partial z} - \rho_1 g \sin\beta \; ; \quad \mu_2 \left(\frac{\partial^2 u_2}{\partial x^2} + \frac{\partial^2 u_2}{\partial y^2} \right) = \frac{\partial P_2}{\partial z} - \rho_2 g \sin\beta \quad (2.1)$$

The required boundary conditions follow from the no-slip condition at the pipe wall and continuity of the velocities and tangential shear stresses across the fluids' interface. For a given axial pressure drop, the solution for u_1 and u_2 can be integrated over the fluids flow cross sections to yield the corresponding volumetric flow rates Q_1 and Q_2. From the practical point of view, we are interested in a solution for the pressure drop and flow geometry (interface location) for given flow rates. However, the inverse problem is much more complicated, since the shape of fluids interface is, in fact, unknown.

2.1 The interface shape

The location of the interface can be obtained by considering the Navier-Stokes equations in the y and x directions:

$$\frac{\partial P_j}{\partial y} + \rho_j \; g\cos\beta = 0 \quad ; \quad \frac{\partial P_j}{\partial x} = 0 \quad ; \quad j = 1,2 \qquad (2.2)$$

Note that equations (2.2) yield $\frac{\partial}{\partial y}\left(\partial P_j/\partial z\right) = 0$ and $\frac{\partial}{\partial x}\left(\partial P_j/\partial z\right) = 0$. Thus, the pressure gradient in the axial direction is the same for the two fluids ($\partial P_1/\partial z = \partial P_2/\partial z = \partial P/\partial z$). Integration of (2.2) in the y direction yields a linear variation of the pressure in this direction due to the hydrostatic pressure:

$$P_1 = P_{1i} - \rho_1 (y-\eta) g\cos\beta \quad ; \; P_2 = P_{2i} - \rho_2 (y-\eta) g\cos\beta \qquad (2.3)$$

where P_{1i}, P_{2i} are the local pressures at either side of the fluids interface, at $y = \eta(x)$. For an axial, fully developed flow, the hydrodynamic stresses normal to the fluids interface vanish. In this case, the equation for the interface location evolves from the condition of equilibrium between the pressure jump across the interface and the surface tension force:

$$P_{1i} - P_{2i} = \frac{\sigma}{R_i} \qquad (2.4)$$

where σ is the surface tension (assumed constant) between the two fluids and R_i is the local radius of the interface curvature:

$$R_i = \left\{ \frac{d}{dx} \frac{d\eta/dx}{[1+(d\eta/dx)^2]^{1/2}} \right\}^{-1} = -\left\{ \frac{d}{d\eta} \frac{dx/d\eta}{[1+(dx/d\eta)^2]^{\frac{1}{2}}} \right\}^{-1} \qquad (2.5)$$

The interfacial curvature in the axial direction is infinite. Equation (2.4) is the well-known Laplace (1806) formula that can be put in the following form:

$$\sigma \frac{d}{dx} \left\{ \frac{d\eta/dx}{[1+(d\eta/dx)^2]^{\frac{1}{2}}} \right\} - (\rho_2 - \rho_1)\eta g\cos\beta = \text{const} = \lambda \qquad (2.6)$$

Equation (2.6) is a non-linear differential equation for $\eta(x)$. Thus, for the flow field under consideration, the position of the fluids interface can be obtained by solving the quasi-static situation. The solution for $\eta(x)$ should comply with the wettability condition at the pipe wall and symmetry with respect to the y axis. It is also constrained by the fluids in-situ holdup available in the flow.

The same differential equation (2.6) can be also obtained from the variational problem of minimizing the total system free energy (Bentwich, 1976, Gorelik and Brauner, 1999). Given the fluids holdup, the components of the free energy, that are subject to variation with changes in the interface shape, are the potential energy in the gravity field and the surface energy (due to the liquids contact with the pipe wall and the liquid-liquid interface). The fact that the same differential equation evolves suggests that the formulation of a variational problem that minimizes the system potential and surface energies is consistent with the hydrodynamic equations for unidirectional and fully developed axial flow. Hence, no other energies (such as the fluids kinetic energies) should be included in the analysis. Equation (2.6) was solved numerically by Bentwich (1976) and analytically by Gorelik and Brauner (1999) and Ng et al., (2001) in terms of elliptical integrals. The analytical solution includes the shape of the interface, $\eta(x)$ and the dimensionless capillary pressure, $\Lambda = 4\lambda/(\Delta\rho g \cos\beta D^2)$, in terms of three dimensionless parameters: the Eotvös number, Eo_D, the fluid/wall wettability angle, α and the fluids holdup. The function $\eta(x)$ determines the geometry of the fluids distribution in the pipe cross section and contact with the pipe wall, whereas Λ is required for calculation of the pressure distribution.

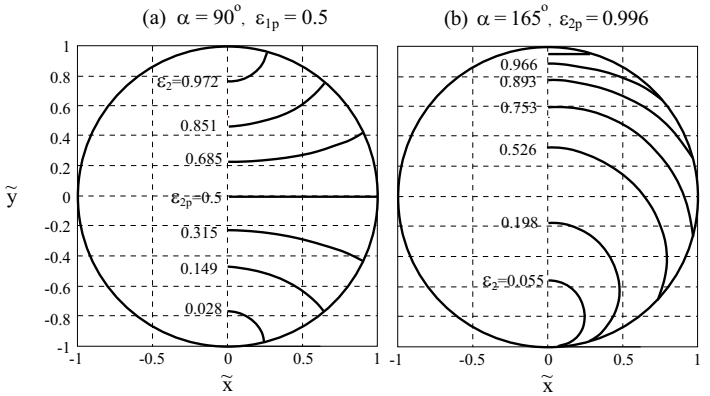

Figure 2.2 Interface configuration for $Eo_D = 1$: effect of holdup for $\alpha = 90^0$ and $\alpha = 165^0$.

An important point to realize is, that in a pipe, the interface shape varies with the fluids holdup. This is demonstrated in Figure 2.2 where the solutions for $\eta(x)$ are given for a constant Eotvös number and different fluids holdup. The case of $\alpha = 90^o$ (Figure 2.2a) corresponds to equal wettability of the two fluids. In this case, the interface is convex for relatively low holdup of the lower phase, $\epsilon_2 < 0.5$ and concave for $\epsilon_2 > 0.5$. For the particular case of $\epsilon_2 = \epsilon_{2p} = 0.5$, the interface is plane, since this configuration satisfies the wettability condition at the solid wall. When the upper phase is the more wetting

phase ($\alpha > 90^o$), ϵ_{2p} increases, as shown in Figure 2.2b (for $\alpha = 165°$, $\epsilon_{2p} \simeq 0.996$). The value of $\epsilon_{1p} = 1 - \epsilon_{2p}$ approaches zero as $\alpha \to \pi$ (ideal wettability of the lighter phase) and the interface is convex independently of the fluids holdup. Similarly, $\epsilon_{2p} \to 0$ as $\alpha \to 0$ and the interface is always concave. However, for partial wettability ($\alpha \neq 0, \pi$), there is a particular value of holdup, ϵ_{1p}, where adhesion forces to the wall are just balanced at the triple point and the system behaves as pseudo gravitational - the interface is plane independently of the Eotvös number. For $\epsilon_2 \neq \epsilon_{2p}$ the interface curvature increases with reducing Eo_D. The dependence of the interface shape on the fluids holdup is a basic difference between pipe flow and channel flow. In a rectangular cross section, the interfacial shape is invariant with the fluids holdup, except for extremely low holdup of one of the phases, where the interface shape may be constrained by the contact with either the upper, or lower wall.

The variation of the TP point location with the holdup and the Eotvös number can be studied in view of Figure 2.3. The location of the TP point corresponding to a plane interface is given by the curve for $Eo_D \to \infty$, when surface forces vanish. The other extreme of no gravity force is described by the curve of $Eo_D = 0$. The figure shows that the location of the TP (represented by ϕ_0) deviates from that predicted by a plane interface (ϕ_0^P) already for $Eo_D = 200$. Figure 2.3a is for almost ideal wettability of the upper phase ($\alpha = 175^0$). For this case $\epsilon_{1p} \to 0$ and the interface is practically convex for any non-vanishing value of the capillary number, $\phi_0 < \phi_0^P$. The effect of Eo_D becomes less pronounced as $\alpha \to 90^0$ (Figure 2.3b).

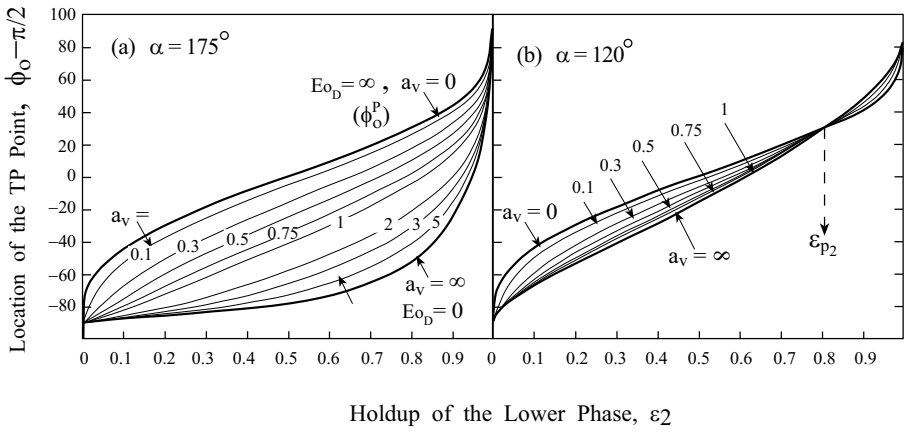

Figure 2.3 The fluids contact with the wall: variation of ϕ_o with the holdup for various Eotvos numbers ($Eo_D = 2/a_v^2$) and wettability anlgles.

2.2 Constant curvature approximation for the interface shape

Exact analytical solutions for the velocity profiles $u_1(x, y), u_2(x, y)$ in laminar flows can be obtained when the fluids interface can be described by a constant curvature curve. In

this case, the bipolar coordinate system can be applied to obtain a complete analytical solution for the velocity profiles, distribution of shear stresses along the pipe wall and fluids interface, axial pressure drop and in-situ holdup, in terms of prescribed flow rates and fluids viscosities (Bentwich, 1964, Brauner et al.,1995, 1996a, Moalem Maron et al., 1995). Otherwise, given the location of the interface $\eta(x)$, numerical schemes must be used for solving the Stokes equations (2.1)(see Ng et al., 2002). The assumption of a constant curvature is trivially satisfied for a zero interfacial surface tension, where $R_i \to \infty$ in eq. (2.4). In this case, the interface is plane with a zero pressure difference across the interface, and the flow geometry can be described by the thickness of the (lower) fluid layer, h (Figure 2.1). Analytical solutions for flow with a plane interface are given in several publications (Semenov and Tochigin 1962, Bentwich 1964, Ranger and Davis 1979, Brauner et al., 1996a). However, in view of eq. (2.6), the assumption of a constant interfacial curvature is evidently also valid when the effect of the gravitational field is negligible, as under microgravity conditions or when $\rho_2 \simeq \rho_1$, whereby $Eo_D \to 0$.

In an attempt to bridge the gap between large and small Eotvös numbers, Brauner et al., (1996b) modelled the shape of the interface by a constant characteristic interfacial curvature. The appropriate characteristic interfacial curvature was derived by formulating the variational problem of minimizing the sum of the system potential (E_p) and surface energies (E_s) with approximate configurations that are described by a priori unknown constant curvature. The curvature and the location of the TP are subject to variations, which are constrained by a prescribed holdup.

In case the interface is of constant curvature, the flow configuration can be described in terms of two variables: ϕ_0 and ϕ^* (Fig. 2.1). The view angle of the interface from a point on the upper wall, ϕ_0 determines the distribution of the two phases over the tube wall. The interface curvature is determined by ϕ^*, which is the view angle of the two triple points (TP) from a point situated on the phases interface. Given ϕ_0 and ϕ^*, geometrical relationships yield the phases flow areas (A_1 and A_2) contact lengths with the tube wall (S_1 and S_2) and interface length, S_i (see Table 2.1). A plan interface is described by $\phi^* = \pi$. Convex interfaces are described by ϕ^* less than π, up to the limit of $\phi^* = 0, \phi_0 = 0$, which corresponds to a fully eccentric core of the lower phase touching the tube bottom. Concave interfaces are described by $\phi^* > \pi$, up to the limit of $\phi^* = \pi \;\; \phi_0 = 2\pi$, which corresponds to a fully eccentric core of the upper phase. It is to be noted that ϕ^* is always bounded between ϕ_0 and $\phi_0 + \pi$.

Taking a configuration of plane interface as a reference, the expression obtained for the system free energy reads:

$$\frac{\Delta\widetilde{E}}{L} = \frac{\Delta Es + \Delta Ep}{LR^3(\rho_2 - \rho_1)g\cos\beta} = \left[\frac{\sin^3\phi_0}{\sin^2\phi^*}(ctg\phi^* - ctg\phi_0)\left(\pi - \phi^* + \frac{1}{2}\sin(2\phi^*)\right)\right.$$

$$\left. + \;\frac{2}{3}\sin^3\phi_0^P\right] + Eo_D^{-1}\left[\sin\phi_0\frac{(\pi - \phi^*)}{\sin\phi^*} - \sin\phi_0^P + \cos\alpha(\phi_0^P - \phi_0)\right] \qquad (2.7)$$

Table 2.1: Geometrical relationships for curved and plane interfaces

	Curved interface, $\phi^* \neq \pi$	Plane interface, $\phi^* = \pi$
$\widetilde{A} = \frac{A}{D^2}$	$\pi/4$	$\pi/4$
$\widetilde{A}_1 = \frac{A_1}{D^2}$	$\frac{1}{4}\left\{\pi - \phi + \frac{1}{2}\sin(2\phi) - \left(\frac{\sin\phi_0}{\sin\phi^*}\right)^2\left[\pi - \phi^* + \frac{1}{2}\sin(2\phi^*)\right]\right\}$	$\frac{1}{2}\left[\pi - \phi_0^P + \frac{1}{2}\sin(2\phi_0^P)\right]$
$\widetilde{A}_2 = \frac{A_2}{D^2}$	$\frac{1}{4}\left\{\phi_0 - \frac{1}{2}\sin(2\phi_0) - \frac{\sin^2\phi_0}{\sin^2\phi^*}\left[\phi^* - \pi - \frac{1}{2}\sin(2\phi^*)\right]\right\}$	$\frac{1}{4}\left[\phi_0^P - \frac{1}{2}\sin(2\phi_0^P)\right]$
$\widetilde{S}_1 = \frac{S_1}{D}$	$\pi - \phi_0$	$\pi - \phi_0^P$
$\widetilde{S}_2 = \frac{S_2}{D}$	ϕ_0	ϕ_0^P
$\widetilde{S}_i = \frac{S_i}{D}$	$(\pi - \phi^*)\sin(\phi_0)/\sin(\phi^*)$	$\sin(\phi_0^P)$
$\widetilde{U}_1 = \frac{U_1}{U_{1S}}$	$\pi/\left\{\pi - \phi_0 + \frac{1}{2}\sin(2\phi_0) - \left(\frac{\sin\phi_0}{\sin\phi^*}\right)^2\left[\pi - \phi^* + \frac{1}{2}\sin(2\phi^*)\right]\right\}$	$\pi/\left[\pi - \phi_0^P + \frac{1}{2}\sin(2\phi_0^P)\right]$
$\widetilde{U}_2 = \frac{U_2}{U_{2S}}$	$\pi/\left\{\phi_0 - \frac{1}{2}\sin(2\phi_0) + \left(\frac{\sin\phi_0}{\sin\phi^*}\right)^2\left[\pi - \phi^* + \frac{1}{2}\sin(2\phi^*)\right]\right\}$	$\pi/\left[\phi_0^P - \frac{1}{2}\sin(2\phi_0^P)\right]$

Given Eo_D, α and $\epsilon_2 = A_2/A$, the equilibrium interface shape is determined by ϕ_0 and ϕ^* which correspond to a minimum of $\Delta\widetilde{E}$ subject to the constraints:

$$\epsilon_2 = \frac{1}{\pi}\left\{\phi_0 - \frac{1}{2}\sin(2\phi_0) + \left(\frac{\sin\phi_0}{\sin\phi^*}\right)^2\left[\pi - \phi^* + \frac{1}{2}\sin(2\phi^*)\right]\right\} \; ; \phi^* \neq \pi$$
$$\epsilon_2 = \frac{1}{\pi}\left[\phi_0^P - \frac{1}{2}\sin(2\phi_0^P)\right] \; ; \phi^* = \pi \tag{2.8}$$

The particular ϕ^* which corresponds to minimal energy is thus a function of the three non-dimensional parameters $\phi^* = \phi^*(Eo_D, \alpha, \text{ holdup}) = \phi^*(Eo_D, \alpha, \phi_0)$. Note that in the approximate solution, the ϕ^* only approximately satisfies the wettability condition. However, in the extremes of $Eo_D = 0$ or $Eo_D \to \infty$, (where also the exact interfacial shapes correspond to a constant curvature) the approximate and exact solutions coincide.

$$\phi^*(\phi_0, \alpha) = \pi \;\Rightarrow\; \text{plane interface}; Eo_D \to \infty$$
$$\phi^*(\phi_0, \alpha) = (\pi - \alpha) + \phi_0; \quad Eo_D \to 0 \tag{2.9}$$

The largest deviations of the approximate solution were obtained for $Eo_D \simeq 0.5 \div 1$ and ideal wettability of either of the phases. However, Figure 2.4a shows that even in this range of parameters, the approximate solution closely follows the exact solution in describing the effect of the holdup on the curving of the interface. Figure 2.4b summaries results for ϕ_o obtained with various wettability angles and shows that the comparison improve as $\alpha \to \pi/2$. The largest deviations are for $\alpha \to 180°$(or $\alpha \to 0°$). However, for $\alpha = 135°$ (or 45°) the differences between the two solutions are already un-noticeable.

The results obtained for the interface shape, which corresponds to minimum energy of eq. (2.7), have been used to construct the so-called 'interface monograms' (Fig. 9 in Brauner, 1998). Given the Eotvös number and the wall/phases adhesion properties as reflected by the wettability angle, a curve relating the interfacial curvature, ϕ^*, to the

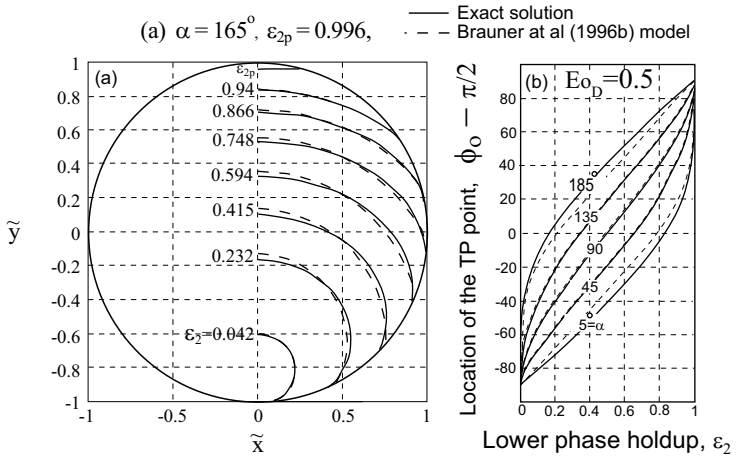

Figure 2.4 Comparison of the characteristic curvature model with the exact solution $Eo_D = 0.5$:
a) curves of $\widetilde{\eta}(x)$ for $\alpha = 165^0$, b) value of ϕ_0 vs. ϵ_2 for various α.

phases distribution angle ϕ_0, is obtained. Each point along an interface monogram is associated with a different holdup. That form of the interface monogram can be conveniently combined with the solution of the flow problem, where the phases in situ holdup is obtained via the solution of the flow equations (see Figure 2.5 below).

2.3 Exact solutions of two-phase laminar pipe flow

The appropriate coordinate system for solving the flow problem, for stratified flow with a curved interface is the well-known bipolar coordinate system. Coordinate ϕ represents the view angle of the two triple points (TP) from an arbitrary point in the flow domain (Figure 2.1). Coordinate ξ relates to the ratio of the radius vectors r_1, r_2 ($\xi = ln(r_1/r_2)$). The pipe perimeter and the interface between the fluids are isolines of coordinates ϕ, so that the upper section of the tube wall bounding the lighter phase is represented by ϕ_o, while the bottom of the tube, bounding the denser phase, is represented by $\phi = \phi_0 + \pi$. The interface coincides with the curve of $\phi = \phi^*$. Thus, the two-phase domains map into two infinite strips in the (ϕ, ξ) domain and are defined by:

$$\begin{aligned} &\text{Upper phase} : -\infty < \xi < \infty \; ; \quad \phi_0 < \phi < \phi^* \\ &\text{Lower phase} : -\infty < \xi < \infty \; ; \quad \phi^* < \phi < \phi_0 + \pi \end{aligned} \tag{2.10}$$

Analytical solutions of the Stokes equations for horizontal stratified flow with an interface of an arbitrary curvature were explored by Brauner et al., (1995, 1996a). In these studies, analytical expressions in terms of Fourier integrals in the bipolar coordinate system were provided for the velocity profiles ($\widetilde{u}_{1,2} = u_{1,2}/U_R$ and the distribution of shear stresses over the tube wall (τ_1, τ_2) and free interface (τ_i) (see also Moalem Maron

et al, 1995):

$$\widetilde{u}_1(\phi,\xi) = 2\sin\phi_0\{\frac{\sin(\phi-\phi_0)}{\cosh\xi-\cos\phi}+2(1-\widetilde{\mu})\frac{\sin(\phi^*-\phi_0)}{\sin(\phi^*)}\int_0^\infty W_{1v}(\omega,\phi)\cos(\omega\xi)d\omega\} \tag{2.11}$$

$$\widetilde{u}_2(\phi,\xi) = 2\widetilde{\mu}\sin\phi_0\{\frac{\sin(\phi-\phi_0)}{\cosh\xi-\cos\phi}+2(1-\widetilde{\mu})\frac{\sin(\phi^*-\phi_0)}{\sin(\phi^*)}\int_0^\infty W_{2v}(\omega,\phi)\cos(\omega\xi)d\omega\} \tag{2.12}$$

where: $U_R = \frac{D^2}{16\mu_1}\,(\frac{-\partial P}{\partial z})$, $\widetilde{\mu} = \mu_1/\mu_2$, and the spectral functions are given by:

$$W_{1v}(\omega,\phi) = \frac{\sinh[\omega(\phi^*-\pi)]}{\psi(\omega)\sinh(\pi\omega)}\;\frac{\sinh[\omega(\phi-\phi_0)]}{\cosh[\omega(\phi^*-\phi_0)]} \tag{2.13}$$

$$W_{2v}(\omega,\phi) = \frac{\sinh[\omega(\phi^*-\pi)]}{\psi(\omega)\sinh(\pi\omega)}\;\frac{\sinh[\omega(\phi-\pi-\phi_0)]}{\cosh[\omega(\phi^*-\pi-\phi_0)]} \tag{2.14}$$

$$\psi(\omega) = \tanh[\omega(\phi^*-\phi_0)] + \widetilde{\mu}\tanh[\omega(\pi+\phi_0-\phi^*)] \tag{2.15}$$

Thus:

$$\widetilde{u}_{1,2} = \frac{u_{1,2}}{U_R} = \widetilde{u}(\phi_0,\phi^*,\widetilde{\mu});\;\widetilde{\boldsymbol{\tau}}_1,\widetilde{\boldsymbol{\tau}}_2,\widetilde{\boldsymbol{\tau}}_i = \widetilde{\boldsymbol{\tau}}(\phi_0,\phi^*,\hat{\mu}) \tag{2.16}$$

where $\widetilde{\tau} = \frac{\tau}{\tau_R}$; $\tau_R = \frac{R}{2}\left(-\frac{\partial P}{\partial z}\right)$. Note that the velocity and shear stress scales used for normalization include the unknown pressure drop. The phases flow rates are obtained by integrating the phases velocities over the corresponding flow areas A_1 , A_2 (see Table 2.1). For a given pressure drop and a viscosity ratio, the integration yields Q_1 and Q_2 as functions of $(\phi_0,\ \phi^*,\ \widetilde{\mu},\ \partial P/\partial z)$. The ratio of the two fluids flow rates, however, is independent of the system pressure drop; $\widetilde{Q} = \frac{Q_1}{Q_2} = \widetilde{Q}(\phi_0,\ \phi^*,\ \widetilde{\mu})$. The corresponding pressure drop (normalized with respect to the superficial pressure drop of the upper fluid) is $\left(\frac{d\widetilde{P}_1}{dZ}\right) = \frac{(-\partial P/\partial z)}{(\partial P/\partial z)_{1S}} = \frac{d\widetilde{P}_1}{dZ}(\phi_0,\ \phi^*,\ \widetilde{\mu})$. Therefore, once the fluids viscosities and flow rates are known, the solution of the flow equations provide a relationship between ϕ_0 and ϕ^*:

$$\phi_0 = \phi_0(\phi^*) \quad\rightarrow\quad \text{Flow Monogram for specified } \widetilde{\mu} \text{ and } \widetilde{Q} \tag{2.17}$$

Once the interface curvature is also specified, for instance, a plane interface ($\phi^* = \pi$), the corresponding ϕ_0 can be obtained, and then the system pressure drop, dimensional velocity profiles and shear stress profiles can be computed. However, the interfacial curvature should comply with the continuity of normal stresses (pressure and surface tension forces) across the interface and with solid/fluids adhesion forces (wettability angle). Hence, the closure relationship needed for the interfacial curvature is provided by the system 'interface monogram' $\phi^* = \phi^*(Eo_D,\alpha,\phi_0)$ as described in Section 2.2.

A convenient frame for obtaining a complete solution (which includes the interface curvature) is via the construction of the system 'operational monograms' (Fig. 2.5). These monograms combine the system 'interface monogram' (dashed curves) with the system

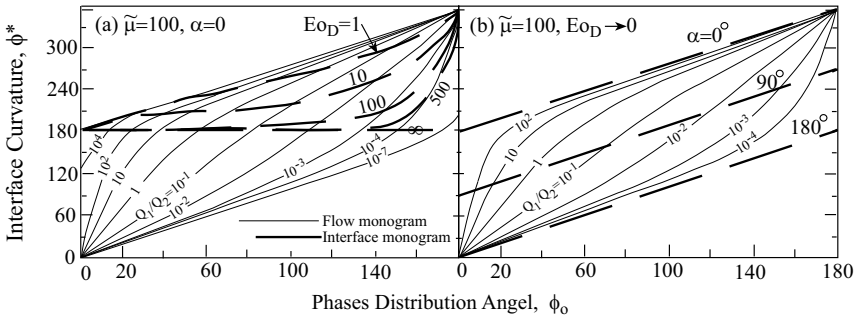

Figure 2.5 Operations monogram - effect of Eotvös number and wettability angle on the stratified flow geometry (ϕ_0 and ϕ^*).

'flow monograms'. The intersection points of the 'interface' and 'flow' monograms represent all stratified flows solutions obtained for various Q_1/Q_2 ratios. Fig. 2.5 indicates that for a given physical system parameters $(\widetilde{\mu}, \alpha, Eo_D)$ and operational conditions Q_1/Q_2, there exists a single solution (ϕ^*, ϕ_0) which determines the resulting flow characteristics. Fig. 2.5a shows that as Eo_D decreases, the solutions for the flow configuration correspond to stratified flow with curved interfaces ($\phi^* \neq 180^0$). The interfacial curvature increases with decreasing Eo_D. Stratified configurations with curved interfaces may also be obtained in systems of low Eotvös number with partial wettability of the fluids (Fig. 2.5b for $0 < \alpha < 180^o$). But, for $Eo_D \to 0$ and ideal wettability of either one of the phases ($\alpha = 0$ or $\alpha = 180^0$ in Fig. 2.5) the solutions obtained correspond to fully eccentric core-annular configuration, irrespective of the phases flow rates (and viscosities). When the upper phase is the wetting phase, $\alpha = 0$, the solution is $\phi_0 = 180^0$, $\phi^* = 360^0$, which corresponds to a fully eccentric core of the upper non-wetting phase touching the upper tube and surrounded by an annulus of the wetting phase. For $\alpha = 180^0$, the solution is $\phi_0 = 0$ and $\phi^* = 0$, in which case the lower phase forms a fully eccentric core at the tube bottom, which is surrounded by the upper wetting phase. Indeed, the occurrence of annular flow in liquid-liquid system is more frequently encountered in oil-water systems of low density differential and small diameter tubes, which are characterized by small Eotvös number.

Exact solutions of the Stokes equations (2.1) for inclined flows assuming a plane interface between the fluids ($\phi^* = \pi$) were obtained by Masliyah and Shook, 1978, Biberg and Halvodsen, 2000 and Goldstein, 2002. These solutions are valid only for large Eo_D systems.

2.4 The two-fluid model (TFM)

For laminar stratified flows, exact solutions of the Stokes equations can be obtained which include the characteristic interface curvature and all the details of the local and integral flow characteristics. But, these analytical solutions still involve extensive computations. In many practical situations, one of the phases (or both) is turbulent. Therefore, for

practical applications, there is a need for a model which can also handle turbulent flows and mixed flow regimes in horizontal and inclined systems. To this end, the two-fluid model can be used (Brauner and Moalem Maron, 1989, Brauner et al., 1998). The model equations presented here and in a unified form that is applicable both to co-current and counter current stratified flows (Ullmann et al., 2002a). Assuming a fully developed flow, the integral forms of the momentum equations for the two fluids are (see Figure 2.1):

$$\begin{aligned} -A_1\left(\frac{\mathrm{d}P}{\mathrm{d}z}\right) + \tau_1 S_1 + \tau_i S_i + \rho_1 A_1 g \sin\beta = 0 \\ -A_2\left(\frac{\mathrm{d}P}{\mathrm{d}z}\right) + \tau_2 S_2 - \tau_i S_i + \rho_2 A_2 g \sin\beta = 0 \end{aligned} \tag{2.18}$$

Eliminating the pressure drop yields:

$$-\tau_1 \frac{S_1}{A_1} + \tau_2 \frac{S_2}{A_2} - \tau_i S_i \left(\frac{1}{A_1} + \frac{1}{A_2}\right) + (\rho_2 - \rho_1)\ g\ \sin\beta = 0. \tag{2.19}$$

The Blassius equation can be used to provide the closure laws required for the wall and interfacial shear stresses ($\tau_1,\ \tau_2,\ \tau_i$) in terms of the average velocities, $U_1,\ U_2$ and the friction factors f_1, f_2 and f_i:

$$\begin{aligned} \tau_1 &= -\frac{1}{2} f_1 U_1 |U_1|; \quad f_1 = C_1 \left(\frac{\rho_1 D_1 |U_1|}{\mu_1}\right)^{-n_1} \\ \tau_2 &= -\frac{1}{2} f_2 U_2 |U_2|; \quad f_2 = C_2 \left(\frac{\rho_2 D_2 |U_2|}{\mu_2}\right)^{-n_2} \\ \tau_1 &= -\frac{1}{2} f_i \rho (U_1 - U_2)|U_1 - U_2| \ . \end{aligned} \tag{2.20}$$

where U_1, U_2 are positive (negative) for downward (upward) flow ($\beta > 0$ in both cases). The Reynolds numbers for the two fluids in eq. (2.20) are based on the equivalent hydraulic diameters, which are defined according to the relative velocity of the phases. In co-current flow, the interface is considered as "free" for the slower phase and as a "wall" for the faster phase. When the velocities are of the same order, the interface is considered "free" with respect to both phases:

$$\begin{aligned} &D_1 = \frac{4A_1}{(S_1 + S_i)}; \ \ D_2 = \frac{4A_2}{S_2}; \ \ \rho = \rho_1 \ \text{ and } \ f_i = F_i f_1 \quad \text{ for } \ |\mathbf{U_1}| > |\mathbf{U_2}|. \\ &D_1 = \frac{4A_1}{S_1}; \ \ D_2 = \frac{4A_2}{(S_2 + S_i)}; \ \ \rho = \rho_2 \ \text{ and } \ f_i = F_i f_2 \quad \text{ for } \ |\mathbf{U_2}| > |\mathbf{U_1}|. \\ &D_1 = \frac{4A_1}{S_1}; \ \ D_2 = \frac{4A_2}{S_2}; \ \ \tau_i \simeq 0 \quad \text{for} \quad \mathbf{U_1} \simeq \mathbf{U_2} \ . \end{aligned} \tag{2.21}$$

In counter-current flow, each of the layers is dragged by the other one opposite to its flow direction, therefore:

$$D_2 = \frac{4A_2}{S_2 + S_1} \quad ; \quad D_1 = \frac{4A_1}{S_1 + S_i} \tag{2.22}$$

A value of $F_i > 1$ can be introduced in eqs. (2.21) to account for a possible augmentation of f_i due to irregularities at the free interface. However, due to the lower density (hence velocity) difference and lower surface tension encountered in liquid-liquid systems, the interface appears less roughened compared to gas-liquid systems. The main issue here concerns the decision as to which of the liquids actually dominates the interfacial interactions. In case of a perturbed interface, the effects of drop entrainment and the consequential mixing at the interface, rather than the wave phenomenon, have to be considered.

Introducing non-dimensional variables (length normalized by D, area by D^2 and velocities by superficial velocities U_{1s}, U_{2s}, see Table 2.1), the various geometric parameters and the non-dimensional velocities $\widetilde{U}_1, \widetilde{U}_2$ are all functions of the phases distribution angle over the tube wall, ϕ_0 and the interface curvature ϕ^*. Given the flow regime in the two-layers ($C_{1,2}$ and $n_{1,2}$ in eq. (2.20) are prescribed), the general relation stated by the dimensionless form of the combined momentum equation (2.19) is:

$$f(\chi^2, \widetilde{Q}, Y, \phi*, \phi_0) = 0 \ ; \quad \text{Flow monogram} \tag{2.23}$$

The three non-dimensional parameters of the solution χ^2, Y and $\widetilde{Q}$, which evolve through the normalization of the combined momentum equation, are given by:

$$\begin{aligned} \chi^2 &= \frac{2C_2/D|\mathbf{U}_{2s}D/\nu_2|^{-n_2}\rho_2|\mathbf{U}_{2s}|}{2C_1/D|\mathbf{U}_{1s}D/\nu_1|^{-n_1}\rho_1|\mathbf{U}_{1s}|}\frac{U_{2s}}{U_{1s}} = \frac{(-dP/dz)_{2s}}{(-dP/dz)_{1s}} \\ Y &= \frac{(\rho_2-\rho_1)g\sin\beta}{2C_1/D|\mathbf{U}_{1s}D/\nu_1)|^{-n_1}\rho_1|\mathbf{U}_{1s}|U_{1s}} = \frac{(\rho_2-\rho_1)g\sin\beta}{(-dP/dz)_{1s}} \ ; \ \widetilde{Q} = \frac{Q_1}{Q_2} = \frac{U_{1s}}{U_{2s}} \end{aligned} \tag{2.24}$$

It is worth noting that for co-current flow U_{1s}, U_{2s} are positive in case of downward flow and are negative both for upward flow, whereas, for counter-current flow U_{1s} is negative, (the light phase flows upward). Therefore, concurrent flows correspond to positive X^2 with $Y > 0$ for down-flow and $Y < 0$ for up-flow. Countercurrent flows correspond to negative X^2 with $Y < 0$. The number of non-dimensional parameters, which eventually define the flow monogram, depend on the flow regime in both phases. In particular, for horizontal laminar (L-L) flows, $Y = O, \chi^2 = (\widetilde{\mu}\widetilde{Q})^{-1}$, and as in the exact solution, the two-fluid flow monogram yields: $\phi_0 = \phi_0(\widetilde{Q}, \widetilde{\mu}, \phi*)$; while for horizontal turbulent (T-T) flows, the solution is also dependent on fluids density ratio, whereby: $\phi_0 = \phi_0(\widetilde{Q}, \widetilde{\mu}, \widetilde{\rho}, \phi*)$. For mixed flow regime in the two layers, more information is needed, which includes the superficial Reynolds number of either one of the phases. In all cases, the closure relation for the interfacial curvature introduces two-additional non-dimensional parameters, the Eotvös number and the wettability angle.

Results of the two-fluid model are demonstrated in Figure (2.6) (see also Brauner et al, 1998). The height of water climbing on the wall, $h_f = 0.5(1-\cos\phi_0)$, and the location of the oil water interface on the tube centerline, $h_0 = 0.5[1-\cos\phi_0+\sin\phi_0\text{ctg}(\phi^*/2)]$, can be computed once ϕ_0 and ϕ^* are known. The latter can be determined by combining the solution of the two-fluid flow equations, as represented by the flow monogram for specified oil and water flow rates, with the interface monogram for $Eo_D = 10, \alpha = 0$. Fig. 2.6 (a and b) shows a comparison between the experimental data for h_f and h_0 and

the predicted values. The gap between h_f and h_o indicates the extent of water climbing over the wall surface. The height of the water film increases with increasing the water rate or reducing the oil rate, whereby the flow configuration gradually approaches a fully eccentric core-annular configuration. Given the flow geometry, the pressure drop can be computed by either of eqs. (2.18). Figure 2.6c demonstrates that the values predicted for the pressure drop are also in a reasonable agreement with the experimental data indicating a water lubrication effect.

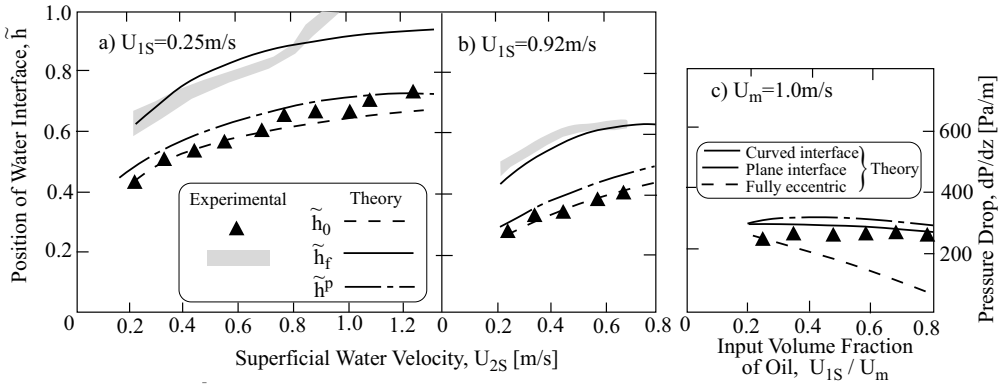

Figure 2.6 Location of the oil-water interface and pressure drop in oil-water system-comparison of the TFM results with Valle and Kvandal (1995) experimental data ($\widetilde{\mu} = 2.26, \widetilde{\rho} = 0.792, Eo_D = 10$, glass tube, $\alpha = 0^0$).

2.5 Two-Plate model (TPM)

Another simple model that can be useful to analyze the characteristics of laminar stratified concurrent and countercurrent inclined flows, however, with a plane interface, is the flow between two parallel plates. For this simple geometry the solution of the Stokes equations (eqs. 2.1) can be easily solved to obtain the velocity profiles. Using mass balances on the two fluids results in the following relations (Ullman et al., 2002a):

$$Y = \frac{1}{4}\frac{(1-\widetilde{h})^2[(1+2\widetilde{h}) + (\widetilde{\mu}-1)\widetilde{h}(4-\widetilde{h})] - \widetilde{h}^2[(3-2\widetilde{h}) + (\widetilde{\mu}-1)\widetilde{h}^2]\widetilde{\mu}\widetilde{Q}}{\widetilde{h}^3(1-\widetilde{h})^3[\widetilde{h}\widetilde{\mu} + (1-\widetilde{h})]\widetilde{\mu}\widetilde{Q}} \tag{2.25}$$

$$\widetilde{P} = \frac{dP/\partial z - \rho_1 g \sin\beta}{(-dP/dz)_{1s}} = \frac{1}{4}\frac{3(1-\widetilde{h})^2 - 4\widetilde{h}(1-\widetilde{h})\widetilde{Q} - \widetilde{h}^2\widetilde{\mu}\widetilde{Q}}{\widetilde{h}(1-\widetilde{h})^2[(1+2\widetilde{h}) + (\widetilde{\mu}-1)\widetilde{h}(4-\widetilde{h}) - 3\widetilde{h}\widetilde{\mu}]\widetilde{Q}} \tag{2.26}$$

where $Y = \frac{(\rho_2-\rho_1)g\sin\beta}{(-dP/dz)_{1s}}$ and $(-dP/dz)_{1s} = 12\mu_1 Q_1/H^3$ is the superficial frictional pressure drop for single phase flow of the lighter phase. Given the parameters Y, $\widetilde{\mu}(=\mu_1/\mu_2)$ and $\widetilde{Q}(=Q_1/Q_2)$, eq. (2.25) can be solved for the *in situ* holdup of the heavier phase $\widetilde{h} = h/H$, which in turn can be substituted in eq. (2.26) to obtain $\widetilde{P}$. The total pressure drop is composed of the gravitational (hydrostatic) pressure drop and the frictional

pressure drop $(dP/dz)_f$:

$$\left(\frac{dP}{dz}\right)_g = [\rho_2\widetilde{h} + \rho_1(1-\widetilde{h})]g\sin\beta = [\rho_1 + (\rho_2-\rho_1)\widetilde{h}]g\sin\beta \tag{2.27}$$

$$\left(\frac{dP_1}{dZ}\right)_f = -\frac{dP/dz - (dP/dz)_g}{(-dP/dz)_{1s}} = -\widetilde{P} + Y\widetilde{h} \tag{2.28}$$

The solution for the holdup vs. the flow rates is demonstrated in Figure 2.7a. This

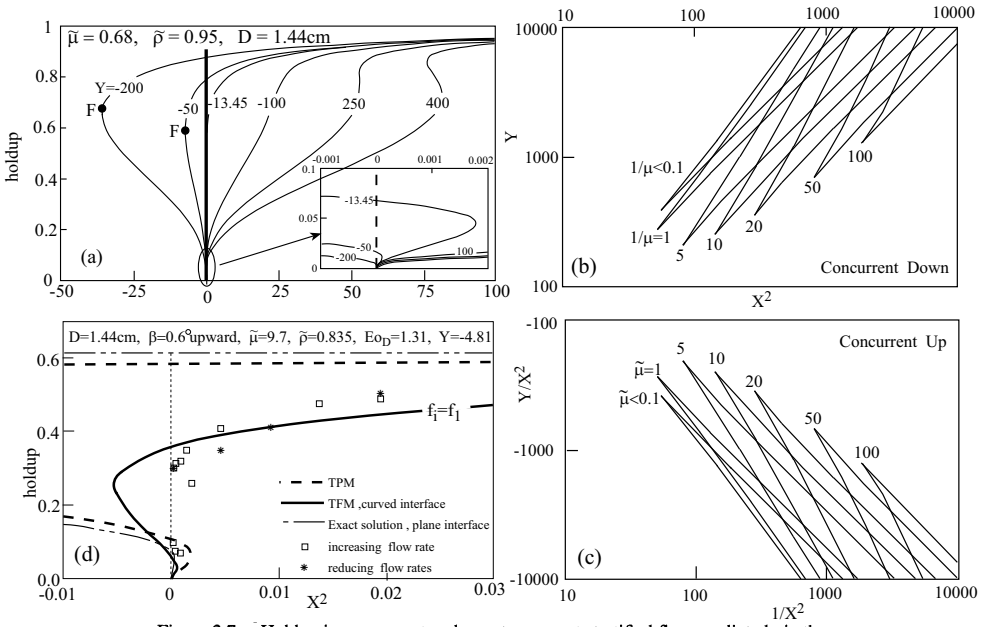

Figure 2.7 Holdup in concurrent and counter current stratified flow predicted via the TPM: (a) Effect of Y, (b,c). Triple solution regions in downward/upward concurrent flows. (d) Experimental verification of multiple holdups.

figure shows the TPM model predictions for the variation of the holdup curves as the inclination parameter changes form a negative to a positive value for a gravity dominated liquid-liquid system ($Eo_D >> 1$) of $\widetilde{\mu} = 0.68, \widetilde{\rho} = 0.95$. For counter-current flows ($\widetilde{Q} < 0$) double holdups are always predicted. Indeed, two-different holdups were observed in experiments on liquid-liquid counter-current stratified flows in inclined columns. These were found to be well predicted by the TPM and TFM models double solutions (Zamir, 2002). Point F represents the ultimate flooding conditions for a specified Y, as there is no solution for counter-current flow beyond this point. In concurrent flow, $\widetilde{Q} > 0$, Figure 2.7a shows that multiple (triple) holdups are predicted by the model in a limited range of operational conditions. Triple solutions for the upward flow ($Y < 0$) are typically obtained for small positive value of $X^2 = (\widetilde{\mu}\widetilde{Q})^{-1}$ corresponding to high flow rates of the light phase and/or low flow rates of the heavy phase (see the detailed picture inserted

in the figure). This figure clearly shows that triple solutions for the holdup are obtained also in downward flows ($Y > 0$). The triple solutions in downward flows are in the range of relatively high X^2 and correspond to relatively high holdups of the heavy phase. These characteristics of the holdup curve in inclined flows are obtained also in the exact solution for laminar flow in inclined pipes (Goldstein,2002) and via the TFM. However, these are much easier to analyze using the TPM.

In view of Figure 2.7a, given a specified value of Y and $\widetilde{\mu}$, the range of $\widetilde{Q}$ corresponding to multiple solutions is bounded by the values of $\widetilde{Q}$ where $d\widetilde{Q}/d\widetilde{h} = 0$. Using eq. (2.25) for calculation of this derivative yields:

$$Y = \frac{1-(\widetilde{\mu}-1)^2\widetilde{h}^4+2(\widetilde{\mu}^2+2\widetilde{\mu}-1)\widetilde{h}^3+(2\widetilde{\mu}-1)\widetilde{h}}{2\widetilde{h}(\widetilde{h}-1)^3[1+(\widetilde{\mu}-1)^2\widetilde{h}^4-2(\widetilde{\mu}-1)(3\widetilde{\mu}-2)\widetilde{h}^3+2(2\widetilde{\mu}^2-6\widetilde{\mu}+3)\widetilde{h}^2+4(\widetilde{\mu}-1)\widetilde{h}]} \tag{2.29}$$

Equations (2.29) and (2.25) can be easily solved simultaneously to yield the X^2 vs. Y relationship that forms the boundaries of multiple solutions regions for a given liquid-liquid system (given $\widetilde{\mu}$). The effect of the viscosity ratio on the range of triple solution in upward concurrent flow is shown in Figure 2.7c in terms of Y/X^2 vs. $1/X^2$. Figure 2.7b is actually its mirror image and represents the ranges where triple solution exists in concurrent downward flows. Figures 2.7(b,c) demonstrate the complete similarity between upward and downward concurrent flows. They also show that there is a minimal X^2 (or minimal $1/X^2$) for concurrent downward (or concurrent upward) flows for which triple solutions can be obtained.

The identification of the parameter space associated with multiple solutions in the exact solution of the Stokes equations (2.1) for pipe geometry, or even in the TFM, requires a tedious search. However, the multiple solutions parameter space in the three models is similar (Goldstein,2002). Hence, the TPM is in fact a useful simple tool for analyzing inclined stratified flows. This model has been used to design an experimental set-up for concurrent upward oil-water flow in the range where multiple configurations are predicted (Gat, 2002). It was verified that multiple holdups are obtained in the experiments (Figure 2.7d), and are not just artifact of the models. Multi-holdups are obviously associated with multi-value pressure drops and other flow characteristics. Therefore, in the range of operational conditions where multiple solutions are suspected, the modelling and design of two-phase flow systems should be approached with extra care. Computational codes usually provide only one solution for specified operational conditions. Therefore, it is necessary to make sure that this solution indeed corresponds to a relevant, physical configuration. Moreover, the possibility of other relevant configurations should be examined. The procedure for using the TPM for identifying the multiple holdups region for turbulent pipe flows of either one of the layers or in both is detailed in Ullmann et al., (2002b).

2.6 Conclusion

The basic configuration in liquid-liquid pipe flow is two-layers separated by a curved interface, rather than a plane interface. Accounting for the interface curvature may have significant effects on the predicted holdup and pressure drop. Exact solutions exist only

for laminar flows. However, the interface curvature can be handled also in the framework of the two-fluid model, which is a useful and simple tool for practical applications. In this model attention must be paid to the closure laws used for the wall and interfacial shear stresses. The two-plates model is a complementary simple tool for analyzing other aspects of liquid liquid inclined flows. In particular, the multi-holdup regions and the characteristic velocity profiles.

3 Core-Annular Flow

One of the flow patterns which appears most attractive from the view point of pressure loss reduction and power saving in the transport of viscous material is that of core annular flow (CAF). The viscous liquid (e.g. heavy crude oil or emulsion, waxy oils) forms the core phase, which is surrounded and lubricated by an immiscible low viscosity liquid (such as water) as the annular phase. A schematic description of CAF is shown in Figure 3.1. A stable CAF is a fully developed flow pattern, where the core and annular phases are distinct and continuous. The continued interest in core-flow resulted in many experimental and theoretical studies, which have been reviewed by Oliemans (1986), Oliemans and Ooms (1986) and Joseph and Renardy (1992). Core flow experiments are summarized in Table 1.2. These experiments proved that if stable core flow can be maintained, the pressure drop is almost independent of the oil viscosity and only slightly higher than for flow of water alone at the mixture flow rate. This flow pattern is promoted by minimizing the density difference between the oil and the lubricating aqueous phase, using additives and surface active agents for controlling and minimizing the emulsification of water into the oil, using hydrophilic pipe material to keep the oil from sticking to the wall and injecting the liquids into the pipe already in this desired configuration.

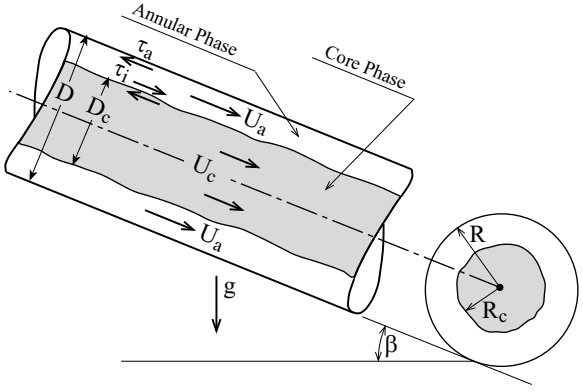

Figure 3.1 Schematic description of core-annular flow configuration.

Due to density difference between the core and annular liquids, the core may stabilize in an off-center position resulting in an eccentric core flow. A steady eccentric core flow is feasible when the overall vertical components of the viscous forces are in a dynamic

equilibrium with the buoyancy force (due to the density differential). Stabilizing hydrodynamic forces may evolve due to core eccentricity and interfacial waviness (Ooms et al., 1984, 1985, Oliemans and Ooms, 1986). The development of a wavy core interface is believed to be a necessary condition for core flow stabilization. However, a critical (minimal) oil superficial velocity and water/oil ratio are required to maintain the core at a sufficiently 'safe' eccentricity, to avoid contamination of the upper tube wall by the waxy oil core. Below a critical oil velocity, a transition to stratified flow takes place with excursion of the pressure drop. The prediction of core-flow boundaries is discussed in Section 5.

3.1 Exact solution for laminar CAF

Models of laminar CAF are relevant for practical applications in particular for the case of CAF of highly viscous oils. The solution of the Stokes equations (2.1) for eccentric core annular flows in horizontal pipes was obtained in terms of Fourier Series in the bipolar coordinate system (Figure 3.2a). When dealing with eccentric core-annular flow, the tube wall is represented by $\xi = \gamma_{\rm w}$, while the two-fluid interface coincides with $\xi = \gamma_c$. Hence, the eccentric core-annular configuration in the x-y domain maps into a semi-infinite strip in the (ϕ, ξ) domain defined by:

$$\begin{aligned} \text{Annular phase}: &\qquad \gamma_{\rm w} < \xi \leq \gamma_c \; ; \quad 0 \leq \phi \leq 2\pi \\ \text{Core phase}: &\qquad \gamma_c < \xi < \infty \; ; \quad 0 \leq \phi \leq 2\pi \end{aligned} \tag{3.1}$$

$$\begin{aligned} \gamma_c &= \cosh^{-1}\left[\frac{(\xi_c+1) - E^2(\xi_c-1)}{2E}\right] \; ; \quad \xi_c = \frac{R}{R_c} \\ \gamma_{\rm w} &= \cosh^{-1}\left[\frac{(\xi_c+1) + E^2(\xi_c-1)}{2E\xi_c}\right] \; ; \quad E = \frac{e/R}{1-1/\xi_c} \end{aligned} \tag{3.2}$$

where R_c is the core radius and e is the core (dimensional) eccentricity. Given the core eccentricity, e, and diameter, R_c, the solution yields the non-dimensional velocity profiles for the core (u_c)and annular (u_a) phases (Bentwich et al., 1970), which can be used to compute the dimensionless wall shear stress and interfacial shear stress profiles:

$$\widetilde{u}_{a,c} = \frac{\widetilde{u}_{a,c}}{U_R} = \widetilde{u}\left(\frac{R_c}{R}, \frac{e}{R}, \widetilde{\mu}\right) ; \;\; \widetilde{\mu} = \frac{\mu_a}{\mu_c}; \;\; U_R = \frac{R^2}{4\mu_a}\left(\frac{-\partial P}{\partial z}\right) \; ; \; \widetilde{\tau}_a, \widetilde{\tau}_i, = \widetilde{\tau}(\widetilde{R}_c, \widetilde{e}, \widetilde{\mu}) \tag{3.3}$$

Integration of the velocity profiles over the phases flow cross section yields:

$$\widetilde{Q} = \frac{Q_a}{Q_c} = \widetilde{Q}(\widetilde{R}_c, \widetilde{e}, \widetilde{\mu}) \; ; \qquad \frac{d\widetilde{P}_c}{dZ} = \frac{(-\partial P/\partial z)}{(-\partial P/\partial z)_{cs}} = \frac{d\widetilde{P}_c}{dZ}(\widetilde{R}_c, \widetilde{e}, \widetilde{\mu}) \tag{3.4}$$

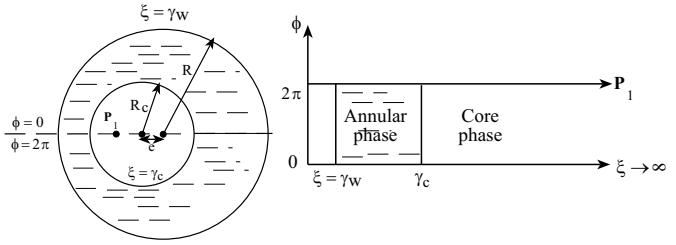

a) Eccentric Core - Annular Flows

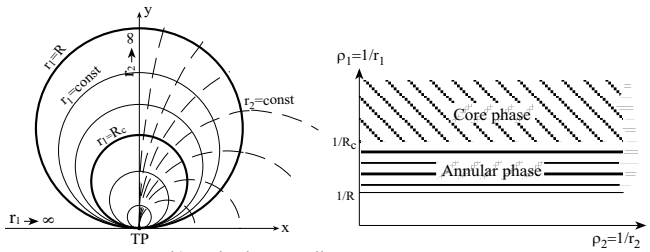

b) Unipolar coordinate system

Figure 3.2 Coordinate systems used to solve the Stokes equations for core flow. (a) Eccentric core-bipolar coordinates. (b) Fully eccentric core-unipolar coordinates.

For concentric core, the solution for eccentric core converges to the simple explicit solution obtained by Russel and Charles, 1959:

$$\frac{\widetilde{A}_c}{1-\widetilde{A}_c} = \frac{1}{\widetilde{\mu}}\left[-1+\left(1+\frac{\widetilde{\mu}}{\widetilde{Q}}\right)^{\frac{1}{2}}\right]$$
$$\frac{d\widetilde{P}_c}{dZ} = \frac{1}{\widetilde{A}_c^2[1+2(\widetilde{A}_c^{-1}-1)/\widetilde{\mu}]} \tag{3.5}$$

which for highly viscous concentric core, $\widetilde{\mu} \ll 1$ yields:

$$\widetilde{D}_c^2 = \widetilde{A}_c = \frac{1}{2\widetilde{Q}+1};\quad \frac{d\widetilde{P}_c}{dZ} = \frac{\widetilde{\mu}(2\widetilde{Q}+1)^2}{4\widetilde{Q}} \tag{3.6}$$

This solution indicates that in the limit of very viscous core flow, the pressure drop reduction factor achieved by the lubricating annular phase is proportional to $\widetilde{\mu}$ ($d\widetilde{P}_c/dZ \to 0$ as $\widetilde{\mu} \to 0$).

But the solution for eccentric core-annular flows fails in the other extreme of fully eccentric core. In this limit, both γ_c and γ_w are zero and the annular phase domain degenerates to a line, $\xi = 0$. The same problem arises when the bipolar coordinates are applied to curved stratified flows. In the limit of a fully eccentric core, the annular phase domain degenerates to an infinite line ($\phi = 2\pi$, for a core of the upper phase, $\phi = 0$ for a core of the lower phase). Thus, the bipolar coordinate system is not appropriate for solving the

flow equations in the limit of a fully eccentric core. When the limit of the fully eccentric core-annular configuration is approached, calculations become tedious. The difficulties have been explained in Rovinsky et al (1997). Typically, the cut-off frequency of spectral functions (needed for carrying out the Fourier integrals in the bipolar coordinate system) is less than 50. However, when a configuration of a fully eccentric core is approached, the cut-off frequency increases by several orders of magnitude. This introduces convergence problems, thus increasing dramatically the computational effort and time. To handle the geometry of a fully eccentric core, a 'unipolar' coordinate system (Fig. 3.2b) has been introduced in Rovinsky et al (1997). Circles of constant r_1 are orthogonal to circles of constant r_2 and all circles are tangent to the single TP. In this coordinate system, the annular phase is described by an infinite strip and a solution for the velocity profiles can be worked out in the form of Fourier integrals. The velocity profiles have been integrated to yield $\widetilde{Q} = \frac{Q_a}{Q_c} = \widetilde{Q}(\widetilde{R}_c, \widetilde{\mu})$; and $\frac{d\widetilde{P}_c}{d\widetilde{Z}} = \frac{(-\partial P/dz)_{TP}}{(-\partial P/dz)_{cs}} = \frac{d\widetilde{P}_c}{d\widetilde{Z}}(\widetilde{R}_c, \widetilde{\mu})$. Given $\widetilde{Q}$ and $\widetilde{\mu}$, the equations are solved to yield $\widetilde{R}_c$ and then the pressure drop, the velocity profiles, as well as wall and interfacial shear stresses profiles for the limit case of fully eccentric core flow were obtained.

Comparison of the analytical solutions for concentric core flow and fully eccentric core flows can be used to evaluate the maximal effect of the core eccentricity on the annular flow characteristics. A detailed discussion has been presented in Rovinsky et al., (1997). Here only some of the results obtained for the effects of core eccentricity are briefly reviewed. Given a flow rate of the viscous phase Q_c(and $\tilde{\mu}$), the introduction of a small amount of the less viscous phase (low Q_a/Q_c) affects initially a decrease of the two-phase pressure drop, where $\frac{(\partial P/\partial z)}{(\partial P/\partial z)_{cs}} = \frac{d\widetilde{P}_c}{d\widetilde{Z}} < 1$. However, eventually, increasing the flow rate of the lubricating phase yields an increase of the pressure drop, where the pressure drop factor exceeds the value of 1.0. The lubrication region is defined by the following range of the Martinelli parameter:

$$\begin{aligned} 0 < \chi^2 = \frac{\mu_a Q_a}{\mu_c Q_c} < 1 \ ; \quad & \text{Concentric core} \\ 0 < \chi^2 < 0.65 \ ; \quad & \text{Fully eccentric core} \end{aligned} \tag{3.7}$$

Thus, the lubrication region is scaled with μ_c; given the flow rate of the viscous phase, Q_c, the range of the flow rates of the less viscous phase, which yields a lubricating effect, increases with increasing the oil viscosity. The potential for pressure drop reduction and power saving in core flows increases with increasing the core viscosity. But, increasing the core eccentricity reduces the potential of pressure drop reduction in lubricated core flow. Figure 3.3c shows that the pressure drop in concentric core-flow is always lower than that obtained with a fully eccentric core. Note that the pressure drop ratio is also the ratio of the pressure drop reduction factor that can be achieved in these two extremes. In concentric core flows, the pressure reduction factor is proportional to $\widetilde{\mu}$, while with a fully eccentric core, the pressure drop reduction factor is bounded (for concentric core: $\frac{d\widetilde{P}_c}{d\widetilde{Z}} \longrightarrow 0$ as $\tilde{\mu} \rightarrow 0$, while for fully eccentric core: $\frac{d\widetilde{P}_c}{d\widetilde{Z}} \longrightarrow 0.025$, see Figure 3.3a). Obviously, the results shown in Figure 3.3 for a fully eccentric core flow provides an upper bound for the effect of core eccentricity.

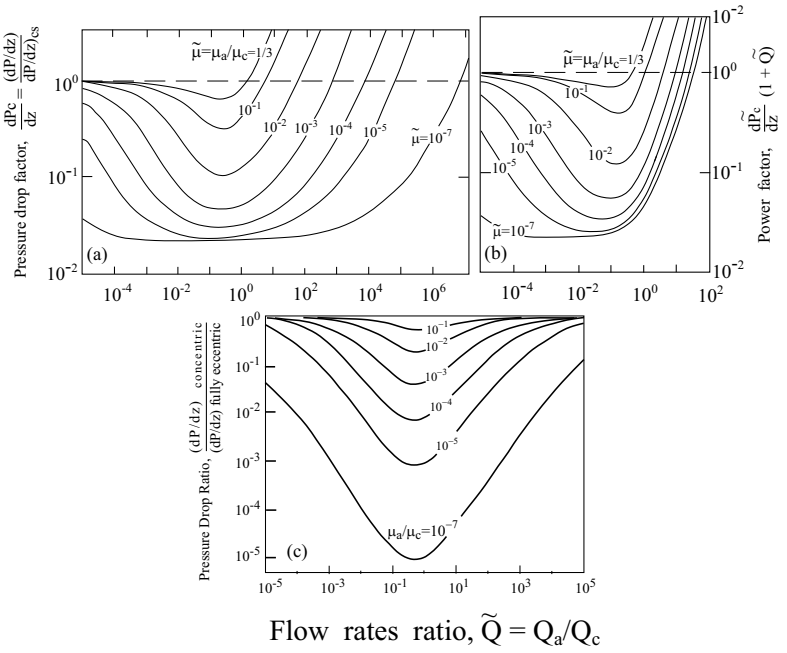

Figure 3.3 The effect of core eccentricity on the potential of pressure drop reduction and power saving in laminar core flow (Rovinsky et al,1997).

The increase of the pressure drop in eccentric core flow evolves from the reduction of the annular-phase holdup and the increase of the wall shear stress. In fact, in concentric viscous core flow, the average velocity of the viscous core phase, U_c always exceeds the average velocity of the lubricating annular phase, U_a: The ratio U_c/U_a approaches a value of 2 for thin annular layer or $\tilde{\mu} \ll 1$. But, when the core approaches a fully eccentric position, it is slowed down (due to the proximity of the tube wall). Consequently, for eccentric core flow, the annular phase velocity may exceed the core phase velocity (for $\tilde{\mu} \ll 1$, the annular phase is the faster phase). As a result, given the flow rates, the viscous core holdup in concentric core flow represents a lower bound for that obtained with the core at eccentric position: $(Ac)_{con}/(Ac)_{ecc} < 1$. However, in the lubrication zone (where $(dP_c/dZ) < 1$), the effect of the core eccentricity on the holdup is moderate ($< 20\%$).

For the opposite case of viscous annulus, $\mu_a/\mu_c > 1$, the effect of core eccentricity on the flow characteristics is moderate. Generally, $(A_c)_{con}/(A_c)_{ecc} < 1$; $(U_c)_{con}/(U_c)_{ecc} > 1$; $(dP/dz)_{con}/(dP/dz)_{ecc} > 1$. The effect of the core eccentricity on the pressure drop is most pronounced around $\chi^2 = \tilde{\mu}\tilde{Q} = 10$, but is limited to about 35% for $\tilde{\mu} \gg 1$.

3.2 Two-Fluid model for CAF

A simple practical model for general annular concurrent liquid-liquid flow, which is not restricted to laminar flow regimes, can be obtained using the two-fluid approach (Brauner,

1991). The combined momentum equation for the core (c) and annular liquid (a) (obtained after eliminating the pressure drop) reads (see Figure 3.1):

$$\frac{4}{D(1-\widetilde{D}_c^2)}\left[-\tau_a+\frac{\tau_i}{\widetilde{D}_c}\right]+(\rho_a-\rho_c)g\sin\beta=0 \tag{3.8}$$

where $\beta>0$ and $\beta<0$ for downward and upward flow, respectively. In core flow $\rho_c=\rho_o$ and $\rho_a=\rho_{\rm w}$, while for the inverted configuration $\rho_a=\rho_o$ and $\rho_c=\rho_{\rm w}$. The wall shear stress τ_a and interfacial shear stress τ_i are expressed in terms of the phases average velocities u_a,u_c and the corresponding friction factors f_a,f_i. The appropriate structure for these closure relations has been identified as (Brauner, 1997):

$$\tau_a=\frac{1}{2}f_a\rho_aU_a^2\quad;\quad f_a=C_a\left[\frac{\rho_aD(1-\widetilde{D}_c^2)U_a}{\mu_a}\right]^{-n_a} \tag{3.9}$$

$$\tau_i=\frac{1}{2}f_i(U_c-c_iU_a)U_c\quad;\quad f_i=F_iC_c\left(\frac{\rho_cD_cU_c}{\mu_c}\right)^{-n_c} \tag{3.10}$$

where $c_i=u_i/U_a$ and u_i is the interfacial velocity. For laminar annular phase $c_i=2$, while for turbulent annular phase $c_i\simeq 1.15\div 1.2$. The constants $C_{a,c}$ and $n_{a,c}$ are set according to the flow regime in each phase ($C=16,\ n=1$ for laminar flow and $C=0.046,\ \ n=0.2$ for turbulent flow). The coefficient F_i denotes possible augmentation of the interfacial shear due to interfacial waviness. However, in core-flow, the liquids interface is characterized by long smooth waves and appears less roughened than in annular gas-liquid flows. Also, as the velocities of the two liquids in core flow are comparable, the modelling becomes even less sensitive to the estimation of the interfacial friction factor, and F_i can be set to 1. Using mass balances on the annular and core phases, $\widetilde{U}_c=\frac{U_c}{U_{cs}}=\frac{1}{\widetilde{D}_c^2}$; $\widetilde{U}_a=\frac{U_a}{U_{as}}=\frac{1}{(1-\widetilde{D}_c^2)}$, results in the following non-dimensional equation for the core diameter:

$$(1-\widetilde{D}_c^2)\widetilde{D}_c^{n_c-5}\left[1-\widetilde{D}_c^2(1+c_i\widetilde{Q})\right]-X^2+Y(1-\widetilde{D}_c^2)^3=0 \tag{3.11}$$

The dimensionless parameters are $\widetilde{Q},\ X^2$ (Martinelli parameter) and Y:

$$X^2=\frac{C_aRe_{as}^{-n_a}}{C_cRe_{cs}^{-n_c}}\frac{\widetilde{Q}^2}{\widetilde{\rho}}=\frac{(dP/dz)_{as}}{(dP/dz)_{cs}}\ ;\ \ Y=\frac{1}{2}\frac{(\rho_a-\rho_c)}{\rho_c}\cdot\frac{Dg\sin\beta}{U_{cs}^2}\frac{1}{C_cRe_{cs}^{-n_c}} \tag{3.12}$$

where $\widetilde{\rho}=\rho_c/\rho_a$ and Re_{as},Re_{cs} are the superficial Reynolds numbers of the annular and core liquids respectively. Obviously the physical solution for $\widetilde{D}_c$ is in the range $0<\widetilde{D}_c\le 1$ and the corresponding core holdup is $\widetilde{A}_c=\widetilde{D}_c^2$. After solving eq. (3.8) for $\widetilde{D}_c$, the pressure gradient can be obtained by adding the momentum equations for the core and annular phases:

$$\frac{d\widetilde{P}_c}{dZ}=\frac{(-dP/dz)}{(-dP/dz)_{cs}}=\frac{X^2}{(1-\widetilde{D}_c^2)^2}-\frac{\rho_m}{\Delta\rho}Y \tag{3.13}$$

where ρ_m is the mixture density; $\rho_m=\rho_c\widetilde{D}_c^2+\rho_a(1-\widetilde{D}_c^2)$.

For viscous oils, the flow in the core is laminar. Fortunately, for the case of horizontal laminar core (with either laminar or turbulent annular phase), simple explicit solutions for the in situ hold-up $\widetilde{D}_c^2$, and the resulting pressure drop are obtained. These are summarized in Table 3.1. Note that the solution obtained for laminar-laminar core flow via the above two-fluid model is identical to the exact solution obtained by Russel and Charles (1959).

For highly viscous oils, $\mu_c/\mu_a >> 1 (X^2 \to 0)$, therefore the predicted insitu holdup is practically determined by the flow rates ratio and flow regime in the annular phase. The data and the model indicate that the water in situ holdup exceeds the input water cut by a few percent (e.g. Figure 12 in Brauner, 1998). Results of pressure drop in CAF are of the order of pressure loss for flow of water at the mixture flow rate (e.g. Figure 13 in Brauner, 1998). Both theory and data indicate that for each oil superficial velocity, there exists an optimum input water-cut (which yields minimum pressure drop) in the range of water-cut of $U_{ws}/U_m = 0.08 \div 0.12$ (compared to an optimal water-cut of 1/3 in L-L flows concentric core flows, e.g Russel and Charles, 1959).

Table 3.1 Core Diameter and Pressure Drop for Laminar Core

	Laminar core - Laminar annulus (L-L)	Laminar core - Turbulent annulus (L-T)
$X^2 =$	$\frac{\mu_a}{\mu_c} \cdot \widetilde{Q}$	$\frac{0.046}{16}\left(\frac{\mu_a}{\mu_c}\right)\widetilde{Q}Re_{as}^{0.8}$ or $\frac{0.046}{16}\left(\frac{\mu_a}{\mu_c}\right)^{0.2}\left(\frac{\rho_a}{\rho_c}\right)^{0.8}Re_{cs}^{0.8}\widetilde{Q}^{1.8}$
c_i	2	$1.15 \div 1.2$
$\tilde{D}_c^2$	$\frac{1+\widetilde{Q}-(1+\widetilde{\mu}/\widetilde{Q})^{1/2}\widetilde{Q}}{1+2\widetilde{Q}-\widetilde{\mu}\widetilde{Q}}$	$\frac{1+\widetilde{Q}c_i/2[1-(1+4X^2/\widetilde{Q}^2c_i^2)^{1/2}]}{1+\widetilde{Q}c_i+X^2}$
$d\widetilde{P}_c/dZ$	$\frac{\widetilde{\mu}}{\widetilde{Q}}\left[\frac{1+2\widetilde{Q}-\widetilde{\mu}\widetilde{Q}}{1-\widetilde{\mu}+(1+\widetilde{\mu}/\widetilde{Q})^{1/2}}\right]^2$	$X^2\left[\frac{1+c_i\widetilde{Q}-X^2}{\widetilde{Q}c_i/2-X^2+(\widetilde{Q}c_i^2/4+X^2)^{1/2}}\right]^2$

3.3 Conclusion

The Two-fluid model for CAF is a simple practical tool for evaluating the potential pressure drop reduction and power saving in concentric CAF. However, the predicted pressure drop via this model may underestimate measured values in CAF operation. Possible reasons for deviations are the increase of the wall friction due to surface irregularities, fouling of pipe walls by a wavy core interface at high oil rates, and eccentric (rather than concentric) core flow, as discussed in Section 3.1. Accounting for these effects in the framework of the two-fluid model requires appropriate modifications of the closure laws used for the wall and/or interfacial shear stresses. The exact solutions for eccentric laminar CAF and numerical studies for the case of turbulent lubricating phase (e.g. Huang et al.,1994) can be used to test the validity of such closure laws.

4 Dispersed Flow

A dispersion of two immiscible liquids, where one of the liquids forms a continuous phase and the other is dispersed in it, is a flow pattern often observed in liquid-liquid systems. There are water-in-oil (w/o) and oil-in-water (o/w) dispersions. Emulsion is a stable dispersion, which usually involves the presence of surfactants that inhibit coalescence of the dispersed droplets. High viscous oil content emulsions are considered a lubricated regime of flow, since a dramatic decrease in the fluid viscosity and pressure drop can be achieved by emulsifying the oil into a continuous water phase, (e.g. McAuliffe, 1973, Pilehvari et al., 1988). Multiple emulsions (e.g. o/w/o, oil drops dispersed in aqueous droplets that are in turn dispersed in a continuous oil phase) can also be formed. Dispersions will always form in motions of two immiscible liquids which are sufficiently intense. However, relatively dilute dispersions can be also obtained at low velocities as a result of the entry device used to introduce the two liquids into the flow tube. In fact, dispersed flow is the basic flow pattern in upward vertical and off-vertical inclined flows.

For fully developed flow, the total pressure gradient, dP/dz is the sum of the frictional pressure gradient, dP_f/dz and the gravitational pressure gradient, dP_g/dz

$$(-dP/dz) = (-dP_f/dz) + (-dP_g/dz) = 2f_m \frac{\rho_m U_m^2}{D} - \rho_m g \sin\beta \tag{4.1}$$

where the z coordinate is attached to the direction of the continuous phase flow, $\beta > 0$ for downward inclination, and the mixture density $\rho_m = \rho_d \epsilon_d + \rho_c(1-\epsilon_d)$ is calculated based on the in situ holdup of the dispersed phase, ϵ_d. The friction factor, f_m is evaluated based on the mixture Reynolds number $DU_m\rho_m/\mu_m$. These require models for the in situ holdup and the mixture apparent viscosity, μ_m. The presence of droplets in a continuous fluid may affect the effective viscosity of the dispersion due to droplets interactions and modification of the continuous phase momentum transfer characteristics.

4.1 In-situ holdup

In vertical and off-vertical inclined systems the static head is a major contributor to the total pressure gradient. Therefore, good estimates for the in situ holdup and the corresponding mixture density are needed.

The simplest approach is the homogeneous model which neglects a possible difference between the in situ velocities of the two liquid phases (slippage). When the dispersed droplets move at the velocity of the surrounding continuous phase, ($U_c = U_d = U_m$), the in situ holdup is determined by the input volumetric flow rates of the two liquids:

$$\epsilon_d = \frac{U_{ds}}{U_m} \quad ; \quad \epsilon_c = 1 - \epsilon_d = \frac{U_{cs}}{U_m} \; ; \; U_m = U_{ds} + U_{cs} \tag{4.2}$$

However, due to the density difference, drops of the dispersed phase tend to move at a different velocity than the continuous phase. The slippage between the phases was found to be negligible for Dw/o in viscous oils or for fine Do/w and Dw/o (e.g. Hassan and Kabir, 1990, Flores et al., 1997). For these flow regimes, the homogeneous model for

estimating ϵ_d, eq. (4.2) is applicable even for inclined and vertical systems. However, when water forms the continuous phase and for low mixture velocities, relatively large oil droplets (bubbles) are formed, which may show a significant slippage.

The Zuber-Findlay (1965) drift flux model can be used to model the flow of oil-in-water dispersions. The average velocity of the dispersed drops, U_d is expressed in terms of the mixture velocity U_m and a drift velocity u_d:

$$U_d = C_o U_m + u_d = U_{ds}/\epsilon_d \quad ; \quad U_c = \frac{U_{cs}}{1-\epsilon_d} \tag{4.3}$$

where C_o is a distribution parameter, which accounts for the droplets velocity and concentration profiles. Typically, $C_o = 1$ for uniform droplet concentration, $C_o > 1$ when the droplets tend to flow at the center and $C_o < 1$ when the droplets concentration is higher near the wall. The drift velocity, u_d is evaluated based on the terminal rise (settling) velocity of a single droplet in the continuous phase, (u_∞) and corrected for the effect of the swarm of drops:

$$u_d = u_\infty (1-\epsilon_d)^{n_d} \mid \sin\beta \mid; \quad 0 < n_d < 3 \tag{4.4}$$

The value of n_d depends mainly on the droplets size. For large drops (of the order of the tube diameter) $n_d \simeq 0$, whereas for liquid-liquid dispersions $n_d = 1.5 \div 2.5$ was recommended by Hassan and Kabir (1990) and Flores et al., (1997).

Equations (4.3) and (4.4) yield an implicit algebraic equation for ϵ_d:

$$\frac{U_{cs}}{U_{ds}} = \frac{1 - C_o\epsilon_d}{C_o\epsilon_d} - \frac{1}{C_o}\frac{u_\infty}{U_{ds}}(1-\epsilon_d)^{n_d} \mid \sin\beta \mid \tag{4.5}$$

This equation is applicable both for concurrent and counter current flows: $U_{cs}/U_{ds} > 0 (< 0)$ for concurrent (counter current) flows, respectively. The sign of u_∞/U_{ds} depends on the direction of u_∞ with respect to U_{ds}. Note that in counter-current flows $u_\infty/U_{ds} > 0$ both for HPD and LPD modes (see Figure 1.3). For $u_d \neq 0$, eq. (4.5) predicts the existence of these two different modes in counter-current dispersed flows.

The drop shape characterization map given in Clift et al., (1978) (see Figure 16 in Brauner, 1998) can be used to extract the drop velocity u_∞. The graphical relation corresponds to $Re_d = Re_d(M,\ Eo_d)$, where $Re_d = \frac{u_\infty d}{\nu_c}$; $M = \frac{g\mu_c^4|\Delta\rho|}{\rho_c^2\sigma^3}$; $Eo_d = \frac{gd^2|\Delta\rho|}{\sigma}$ and d is the drop diameter. Recommended correlations u_∞ are also summarized in this reference. A widely used equation for u_∞ is the Harmathy's (1960) model for distorted drops:

$$u_\infty = 1.53\left[\frac{g\sigma|\Delta\rho|}{\rho_c^2}\right]^{1/4}, \tag{4.6}$$

which suggests u_∞ is independent of the drop diameter. It reflects an increase of the drag coefficient with an increase of the effective cross section of a distorted drop. For large drops, $d/D = O(1), u_\infty$ should be corrected for the reduction of the drop velocity due to pipe wall effects (Clift et al., 1978). For $d/D \simeq 1$ (large bubble or slug) and $Eo_d < 0.125$, $u_\infty \approx 0$, (Zukowski, 1966). Note that in concurrent flows, the sign of u_∞ is to be adjusted according to the sign of the buoyant force due to $\Delta\rho = (\rho_d - \rho_c)g\sin\beta$ with respect to the mixture flow direction. In counter-current flows, the sign of u_∞ is the same as U_{ds}.

4.2 Viscosity of emulsions

When the slippage between the dispersed and the continuous phase is significant, or in coarse dispersions, the mixture viscosity is normally taken as the viscosity of the continuous phase, $\mu_m = \mu_c$. On the other hand, a fine dispersion, or an emulsion, can be treated as a pseudo-homogeneous fluid of a viscosity μ_m, when $Re_c(d/D)^2\rho_d/\rho_c < 1, Re_c = \rho_c U_m D/\mu_c$ (e.g. Baron et al., 1953). Models for estimating the drops size are given in Section 4.4.

The viscosity of emulsion μ_m is defined as the ratio between the shear stress (τ) and the shear rate ($\dot{\gamma}$). The viscosity of the emulsion is proportional to the viscosity of the continuous phase μ_c. However, the emulsion viscosity depends upon several other factors, which include the volume fraction of the dispersed phase (ϵ_d), the droplets size (d) and viscosity (μ_d), the shear rate ($\dot{\gamma}$), temperature (T), the emulsifying agent used and its concentration (e.g Sherman, 1968, Schramm, 1992). At low to moderate holdup of the dispersed phase, emulsions generally exhibit Newtonian behavior.

The emulsion viscosity is affected mainly by the viscosity of the continuous phase and increases with increasing the holdup of the dispersed phase. Following Einstein's relation (1906) for the viscosity of suspensions in extreme dilution:

$$\mu^* = \frac{\mu_m}{\mu_c} = (1 + 2.5\epsilon_d); \quad \epsilon_d \ll 1, \tag{4.7}$$

other models/correlations which relate the emulsion viscosity to the volume fraction of the dispersed phase have been proposed in the literature, in the form of $\mu^* = f(\epsilon_d)$ or $\ln \mu^* = f(\epsilon_d)$. These include empirical fitting constants. A summary of various correlations for μ^* is given in Brauner, 1998, Tables 3a and 3b. In the presence of emulsifiers and/or impurities, the dispersed droplets behave like rigid particles and the emulsion viscosity is independent of the dispersed phase viscosity. In their absence, however, possible internal circulation within the droplets results in some decrease of the emulsion viscosity with reducing the dispersed phase viscosity. For high emulsion concentrations, the empirical correlations use a reduced dispersed phase concentration, $\epsilon_d/\hat{\epsilon}_d$, where $\hat{\epsilon}_d$ represents the maximum attainable dispersed phase concentration at phase inversion. This introduces in the correlations effects of additional parameters, such as emulsifier concentration, flow field and droplets sizes.

At high dispersed phase concentrations (approaching phase inversion conditions) emulsions behave as non-Newtonian shear-thinning (pseudoplastic) fluids (e.g. Pal, 1990). The relation between the shear stress and shear rate is modeled by the power law equation, (in terms of two constants k and n):

$$\tau = -k\dot{\gamma}\left[\dot{\gamma}^{n-1}\right]; \quad n < 1 \tag{4.8}$$

which indicates that the apparent emulsion viscosity $\mu_m = \tau/\dot{\gamma}$ decreases with increasing the shear rate. Concentrated emulsions can also exhibit a viscoelastic behavior.

The viscosity of emulsions decreases with increasing the temperature, $\mu_m = Ae^{-B/T}$, where T is the absolute temperature and A, B are constants dependent upon the specific emulsion and shear rate. Due to the sensitivity of the oil viscosity to temperature

variations, the viscosity of Dw/o and the associated pressure drop are mostly affected by temperature.

Emulsion rheology may vary between different oils and emulsifiers. Even oils of similar properties may exhibit a different emulsion rheology. Therefore, it is recommended to experimentally study the rheology of the emulsion used in a particular application.

4.3 Friction factor

Given the mixture properties, one can apply the single phase flow equations. For laminar flow of Newtonian fluid - the friction factor is obtained from the Hagen-Poiseuille equation:

$$f_m = \frac{16}{Re_m} \quad ; \quad Re_m = \frac{\rho_m U_m D}{\mu_m} \leq 2100 \tag{4.9}$$

For turbulent flow of Newtonian fluids, the friction factor can be obtained from the Moody diagram, or calculated from one of the experimental correlations suggested in the literature. For instance, in smooth tubes, the Blasius correlation is applicable:

$$f_m = \frac{0.079}{Re_m^{0.25}} \; ; \quad 300 \leq Re_m \leq 100,000 \tag{4.10}$$

For rough walls, the Colebrook (1939) equation yields:

$$\frac{1}{\sqrt{f_m}} = -4 \log_{10} \left(\frac{k^*}{3.71} + \frac{1.26}{Re_m \sqrt{f_m}} \right) \tag{4.11}$$

where $k^* = k/D$ is the nondimensional wall roughness scale. An explicit approximation to eq. (4.11) can be used (Zigrang and Sylvester, 1985):

$$\frac{1}{\sqrt{f_m}} = -4 \log_{10} \left[\frac{k^*}{3.71} - \frac{4.518}{Re_m} \log \left(\frac{6.9}{Re_m} + \left(\frac{k^*}{3.7} \right)^{1.11} \right) \right] \tag{4.12}$$

For dense emulsions that behave as non-Newtonian pseudoplastic fluid, the frictional pressure drop can be estimated using Dodge and Metzner (1959) correlations:

$$f_m = \frac{16}{R\acute{e}_m} \quad ; \quad R\acute{e}_m = \frac{\rho_m U_m^{2-n'} D^{n'}}{k' (8)^{n'-1}} \quad ; \qquad \text{laminar flow, } R\acute{e}_m \leq R\acute{e}_{L-T} \tag{4.13}$$

$$\frac{1}{\sqrt{f_m}} = \frac{4}{(n')^{0.75}} \log[R\acute{e}_m f_m^{(1-n'/2)}] - \frac{0.4}{n'^{1.2}} \quad ; \qquad \text{turbulent flow, } R\acute{e}_m > R\acute{e}_{L-T}$$

where $n' = n \leq 1$, $k' = k \left(\frac{1+3n}{4n} \right)^n$ and $n,\ k$ are the constants of the power-law model for the emulsion viscosity (eq. 4.8). The laminar-turbulent transitional Reynolds number is given by $R\acute{e}_{L-T} = 6464 \; \frac{n(2+n)^{\frac{2+n}{1+n}}}{(1+3n)^2}$ (e.g. Hanks and Christeansen, 1962).

The variation of the pressure drop with the liquids flow rates is, however controlled by the phase inversion phenomenon (e.g. Figure 15 in Brauner, 1998). A sudden increase

in the apparent dispersion viscosity (up to one order of magnitude higher than the single phase oil viscosity) occurs where the external phase invert from oil to water (or vice versa). When water forms the continuous phase, the mixture viscosity approaches the single phase water viscosity. The increase of the apparent mixture viscosity at phase inversion (compared to the pure oil viscosity) seems to be moderated with increasing the oil viscosity. The conditions under which phase inversion takes place are discussed in Section 4.5.

4.4 Drops sizes

The mechanisms of drop formation and their characteristic size are important for analyzing the hydrodynamic and transport phenomena in the flow of liquid-liquid dispersions. The main breakup mechanisms involve high shear stresses, turbulence in the continuous phase and rapid acceleration (Taylor, 1934, Kolmogorov, 1949, Hinze, 1955, 1959). The surface force which resists deformation and breakup is mainly due to surface tension and also due to internal viscous force (in the case of viscous drop). In dense dispersions, droplets coalescence and additional factors introduced when a swarm of droplets interact must be taken into account. These lead to an increase of the drop size.

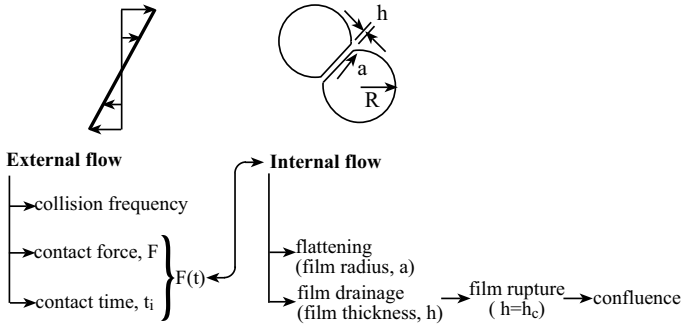

Figure 4.1 Conceptual framework for coalescence modeling (Chesters, 1991).

A substantial effort has been made to model the phenomenon of droplets coalescence in dense dispersions. Reviews of existing frameworks for analysis of droplets interactions with themselves and with the surrounding fluid can be found in Chesters (1991), Tsouris and Taularides (1994). Coalescence actually involves a number of coupled sub-processes (see Figure 4.1). Some are governed by the external flow field, due to the flow of the continuous phase (e.g. frequency of drops collisions, force and duration of collisions). These provide the boundary conditions for the internal flow (i.e. drop deformations, film drainage and rupture of the interfaces). However, the relationships that have been proposed for the various sub-processes involved include unknown parameters and therefore, at this time, they cannot be readily applied to general liquid-liquid flow systems.

In dilute dispersions, however, the characteristic drop size is governed by the drop breakup mechanism. In the following, models for evaluating the maximal drop size associated with the various breakup mechanisms and some extensions to dense dispersions are briefly reviewed. The maximum drop size, $d_{\max}$ provides an estimate to the drop

volume-surface mean size (the Sauter mean diameter) $d_{32} = \sum n_i d_i^3 / \sum n_i d_i^2 \simeq d_{\max}/k_d$ with $k_d \simeq 1.5 \div 3$ (see also Azzopardi and Hewitt, 1997).

Shear flow – Drops deformation and splitting under the action of viscous shear (Couette flow and plane hyperbolic flow) was studied by Taylor (1934). The critical Weber number, defined based on the maximum velocity gradient in the flow field, $We_{crit} = \mu_c \dot{\gamma}_{\max} d_{\max}/\sigma$, was found to vary with μ_d/μ_c. It increases for $\mu_d/\mu_c \gg 1$ or $\mu_d/\mu_c \ll 1$. For $\mu_d/\mu_c \geq 20$ and Couette flow, breakup of drops was not observed. This evidence implies that it is difficult to disperse fluids of high viscosity ratio by the action of viscous shear.

For the case of viscous continuous phase, where $\mu_d/\mu_c \ll 1$, the model of Taylor (1934) and Arivos (1978) for breakup of long slender droplets in an axisymmetric straining motion can be used to estimate the drop size. When applied to laminar pipe flow, where the average value of $\dot{\gamma}$ is given by $\dot{\gamma} = 4U_m/D$, this model suggests that the drop size depends on the capillary number of the continuous phase, $\mu_c U_m/\sigma$:

$$\frac{d_{\max}}{D} = 0.296 \frac{\sigma}{\mu_c \dot{\gamma} D} \left(\frac{\mu_c}{\mu_d}\right)^{1/6} = 0.074 \ \frac{\sigma}{\mu_c U_m} \ \left(\frac{\mu_c}{\mu_d}\right)^{1/6} \ ; \ \frac{\mu_d}{\mu_c} \ll 1 \tag{4.14}$$

Turbulent flow – Most of the models for predicting the size of bubbles or drops in a turbulent flow field are based on the Kolmogorov (1949)-Hinze (1955) model for emulsification in a turbulent flow field. Using dimensional arguments, they showed that the splitting of a drop depends upon a critical Weber number, which yields the maximal drop size, $d_{\max}$ that can resist the stress due to dynamic pressure of turbulent eddies (τ). According to Hinze (1955):

$$We_{crit} = \frac{\tau d_{\max}}{\sigma} = C[1 + F(On)] \tag{4.15}$$

where C is a constant, On is the Ohnesorge (viscosity) number (ratio between the internal viscosity force and the interfacial force); $On = \frac{\mu_d}{\sqrt{\rho_d d_{\max} \sigma}}$ and F is a function that goes to zero as $On \to 0$. For pipe flow of a dilute dispersion, this model yields the maximal drop/bubble size, $d_{\max}$ in terms of the critical Weber number of the continuous phase, $We_c = \rho_c U_c^2 D/\sigma$ and the wall friction factor, f (e.g. Kubie and Gardner, 1977):

$$\left(\widetilde{d}_{\max}\right)_o = \left(\frac{d_{\max}}{D}\right)_o = 0.55 We_c^{-0.6} f^{-0.4} \quad ; \quad \ell_k \ll d_{\max} < 0.1D \tag{4.16}$$

where ℓ_k is the Kolmogorov microscale and 0.1D represents the inertial subrange scale (length scale of energy containing eddies).

The Hinze model is applicable for dilute dispersions. It suggests that the maximal drop size, $(d_{max})_o$, can be evaluated based on a static force balance between the eddy dynamic pressure and the counteracted surface tension force (considering a single drop in a turbulent field). An extension of this model for dense dispersions was suggested by Brauner (2001). The idea is that in dense dispersions, where local coalescence is prominent, the maximal drop size, $(d_{max})_\epsilon$, is evaluated based on a local energy balance.

In the dynamic (local quasi-steady) breakage/coalescence processes, the turbulent kinetic energy flux in the continuous phase should exceed the rate of surface energy generation that is required for the renewal of droplets in the coalescing system. This energy balance yields:

$$\left(\tilde{d}_{max}\right)_\epsilon = \left(\frac{d_{\max}}{D}\right)_\epsilon = 2.22\tilde{C}_H \left(\frac{\rho_c U_c^2 D}{\sigma}\right)^{-0.6} \left[\frac{\rho_m}{\rho_c(1-\epsilon_d)} f\right]^{-0.4} \left(\frac{\epsilon_d}{1-\epsilon_d}\right)^{0.6} \quad (4.17)$$

where $\tilde{C}_H$ is a tunable constant, $\tilde{C}_H = O(1)$. In dilute systems, the energy balance is trivially satisfied for any finite drop size (as the rate of surface energy generation vanishes for $\epsilon_d \to 0$) thus, $(d_{max})_\epsilon < (d_{max})_o$. However, this is not the case in the dense system, where $(d_{max})_\epsilon > (d_{max})_o$. Thus, given a two-fluid system and operational conditions, the maximal drop size is taken as the largest of the two values:

$$\tilde{d}_{\max} = Max\left\{\left(\tilde{d}_{\max}\right)_o \left(\tilde{d}_{\max}\right)_\epsilon\right\} \quad (4.18)$$

Correlations for the friction factor in smooth or rough conduits can be used in eqs. (4.16) and (4.17). For instance, the Blasius equation ($f = 0.046/Re_c, Re_c = \rho_c D U_c/\mu_c$) yields:

$$\left(\frac{d_{\max}}{D}\right)_o = 1.88 We_c^{-0.6} Re_c^{0.08} \quad ; \quad (4.19)$$

$$\left(\tilde{d}_{max}\right)_\epsilon = 7.61\tilde{C}_H We_c^{-0.6} Re_c^{0.08} \left(\frac{\epsilon_d}{1-\epsilon_d}\right)^{0.6} \left[1 + \frac{\rho_d}{\rho_c}\frac{\epsilon_d}{1-\epsilon_d}\right]^{-0.4} \quad ; \quad (4.20)$$

Eqs. (4.18) to (4.20) are the H-model in Brauner (2001), which is applicable provided $1.82 Re_c^{-0.7} < \tilde{d}_{max} < 0.1$ and $Re_c > 2100$.

If the viscosity of the dispersed phase is much larger than that of the continuous phase, the viscous forces due to the flow inside the drop also become important and the effect of the On number in eq. (4.15) may turn to be non-negligible. Kolmogorov (1949) found that when $\mu_d/\mu_c \gg 1$, these viscous forces can be neglected only when $d_{max} \gg \ell_k(\nu_d/\nu_c)^{3/4}$. A correlation for $d_{\max}$, which accounts for viscous forces in the dispersed and continuous phase was suggested by Paul and Sleicher (1965):

$$\frac{\rho_c U_c^2 d_{\max}}{\sigma}\left(\frac{\mu_c U_c}{\sigma}\right)^{0.5} = C\left[1 + 0.7\left(\frac{\mu_d U_c}{\sigma}\right)^{0.7}\right] \quad (4.21)$$

with $C = 38 \div 43$. This correlation indicates no effect of the pipe diameter. Kubie and Gardner (1977) showed that a major part of Sleicher and Paul (1965) data correspond to drops that are larger than the scale of energy containing eddies ($\approx 0.1D$ for pipe flow). It was argued that for $d_{\max} > 0.1D$, the turbulent dynamic pressure force in Kolmogorov/Hinze analysis should be evaluated based on the fluctuating turbulent velocity ($\simeq 1.3u^*$ in pipe flow, Hughmark, 1971). In this case, the correlation that evolves for $d_{\max}$ (instead of eq. (4.16)) reads:

$$\frac{d_{\max}}{D} = 1.38\left(\frac{\rho_c u_c^2 D}{\sigma}\right)^{-1} f^{-1} \quad ; \quad d_{\max} > 0.1D \quad (4.22)$$

Accordingly, for $\widetilde{d}_{\max} > 0.1$, eqs. (4.19 - 4.20) are replaced by the K-Model in Brauner (2001):

$$\left(\widetilde{d}_{\max}\right)_0 = 30We_c^{-1}Re_c^{0.2} \ ; \ \widetilde{d}_{\max} > 0.1 \tag{4.23}$$

$$\left(\widetilde{d}_{\max}\right)_\epsilon = 174C_K We_c^{-1}Re_c^{0.2} \quad \left(\frac{\epsilon_d}{1-\epsilon_d}\right) \ ; \tag{4.24}$$

where $C_K = O(1)$. However, in $D_{\mathrm{o/w}}$ of viscous oils, or in systems of low surface tension, additional stabilizing force due to the drop viscosity has to be considered, which affects an increase of $d_{\max}$ with μ_d. According to Hinze (1955), the effect of the dispersed phase viscosity is represented by the Ohnesorge number. For a non-vanishing On, the r.h.s. of eqs. (4.16) to (4.20) and (4.22)-4.24) are augmented by the term $[1+F(On)]^{0.6}$. Instead, the correction suggested by Davies (1987) can be applied by multiplying the R.H.S. of these equations by $(1+K_\mu \mu_d u_c'/\sigma)^{0.6}$, with $K_\mu = O(1)$, where u_c' is the characteristic turbulent fluctuation velocity in the continuous phase.

Accelerated Drops – Drops deformation and breakup due to rapid acceleration of drops bursting into a stream of a second fluid is the main mechanism for pneumatic atomization and has been studied extensively in the literature (e.g. Hinze, 1955, Clift et al., 1978, Brodkey, 1969, Cohen, 1991). This mechanism can be relevant to the formation of liquid dispersions in the entry region of the pipe, in particular, when nozzles are used for injection of the liquid, or for drop entrainment from the interface between a slow and a fast moving layers (as in wavy stratified flow). The following power-law empirical correlation for We_{crit} is often used to evaluate $d_{\max}$:

$$We_{crit} = \frac{\rho_c \Delta U_c^2 d_{\max}}{\sigma} = 12\left(1+1.077On^{1.6}\right) \tag{4.25}$$

When ΔU_c is set to the initial velocity difference (between the drop and the continuous phase), eq. (4.25) may underestimate $d_{\max}$. Modified correlations which consider the breakup time and velocity history are given in the literature (see review by Azzopardi and Hewitt, 1997).

Rising (settling) drops – Even in a stagnant fluid ($U_c \to 0$), there is a limit to the size to which a bubble or a drop can reach while rising (or falling) freely through it. In the absence of external field disturbances, drop breakup has been attributed to Rayleigh-Taylor instability. Grace et al., (1978) showed that for $\mu_d/\mu_c > 0.5$, $d_{\max} = 4\sqrt{\sigma/g \mid \rho_c - \rho_d \mid}$ provides a reasonable estimate for the maximal drops size. For $\mu_d/\mu_c < 0.5$, it provides a lower bound to $d_{\max}$. Combining the Rayleigh-Taylor instability and Kelvin-Helmholtz instability (Kitsch and Kocamustafaogullari, 1989), the following equation was obtained for $d_{\max}$ of rising (falling) drops in stagnant fluids:

$$d_{\max}\sqrt{\frac{g \mid \rho_c - \rho_d \mid}{\sigma}} = \left\{ \frac{16}{1+0.5\left[4.5\left(\frac{\rho^*}{1+\rho^*}\right) - 0.35\left(\frac{2+3\rho^*}{1+\rho^*}\right)^{2.27}\left(1+M^{0.25}\right)^{0.36}\right]} \right\}^{1/2} \tag{4.26}$$

where $\rho^* = 0.993\rho_d/\rho_c$ and the Morton number, $M \leq 16$. Equation (4.30) predicts the experimentally observed increase of $d_{\max}$ with increasing M. Eq. (4.26) (with a lower numerical coefficient) represents the scale of highly deformable drops/bubbles in vertical and horizontal flows (Brodkey, 1969, Brauner and Moalem Maron, 1992c).

4.5 Phase inversion

The phase inversion refers to a phenomenon where with a small change in the operational conditions, the continuous and dispersed phase spontaneously invert. For instance, in oil-water systems, a dispersion (emulsion) of oil drops in water becomes a dispersion (emulsion) of water drops in oil, or vice versa.

The phase-inversion is a major factor to be considered in the design of oil-water pipelines, since the rheological characteristics of the dispersion and the associated pressure drop change abruptly and significantly at or near the phase inversion point (Pan et al (1995), Angeli and Hewitt (1996), Arirachakaran et al (1989)). Also, the corrosion of the conduit is determined to a large extent by the identity of the phase that wets it.

The inversion point is usually defined as the critical volume fraction of the dispersed phase above which this phase will become the continuous phase. Studies have been carried out in batch mixers, continuous mixers, column contractors and pipe flow, in attempt to characterize the dependence of the critical volume fraction on the various system parameters, which include operational conditions, system geometry and materials of construction. These have been reviewed by Yeo et al., 2000. In flow systems, phase inversion will not always occur as the holdup (say of water) is varied continuously from 0 to 1. It will occur only if U_m is high enough to have a good mixing of the liquids in both the pre- and post inversion dispersions.

Similarly to observations made in stirred tanks, also in pipe flows, data on dispersion inversion indicate a tendency of a more viscous oil to form the dispersed phase. It was found that the water-cut required to invert a dispersion decreases as the oil viscosity, μ_o increases. Based on the experimental results of various investigators on phase inversion, Arirachakaran et al (1989) proposed the following correlation for the critical water-cut, $\dot{\epsilon}_{\mathrm{w}}^I$:

$$\dot{\epsilon}_{\mathrm{w}}^I = \left(\frac{U_{\mathrm{ws}}}{U_m}\right)_I = 0.5 - 0.1108 \log_{10}\left(\mu_o/\mu_r\right);\ \mu_r = 1mPa \cdot s \tag{4.27}$$

The trend is similar to that indicate by the Yeh et al (1964) model for the phase inversion point: $\epsilon_{\mathrm{w}}^I = \frac{1}{1+(\mu_o/\mu_{\mathrm{w}})^{0.5}}$. The later was developed with reference to a configuration of laminar flow in stratified layers, however, its validity was tested against the critical holdup data obtained in a flask (dispersion prepared by manual vigorous shaking of specified volumes of an organic and water phases).

Since phase inversion is a spontaneous phenomenon, it was proposed that its prediction can be based on the criterion of minimization of the total system free energy, (e.g. Luhning and Sawistowski 1971, Tidhar et al., 1986, Decarre and Fabre, 1997, Brauner and Ullmann, 2002). Under conditions where the composition of the oil and water phases and the system temperature are invariant with phase inversion, only the free energies of the interfaces have to be considered. The application of this criterion is, however, dependent on the availability of a model for characterizing the drop size in the initial and

post-inversion dispersions, both are usually dense. This approach was recently followed by Brauner and Ullmann (2002).

According to this approach, when a dispersion structure (say $D_{\mathrm{o/w}}$) is associated with higher surface energy than that obtained with an alternate structure (say $D_{\mathrm{w/o}}$), it will tend to change its structure, and eventually to reach the one associated with the lowest surface energy. Hence, the phase inversion is expected under the critical conditions where both $D_{\mathrm{o/w}}$ and $D_{\mathrm{w/o}}$ are dynamically stable and the sum of surface energies obtained with either of these two configurations are equal.

Based on these considerations, the critical oil holdup can be obtained in terms of the liquid-solid surface wettability angle, α, and the Sauter mean drop diameter in pre-and post inversion dispersions (Brauner and Ullmann, 2002):

$$\epsilon_o^I = \frac{[\sigma/d_{32}]_{\mathrm{w/o}} + \frac{s}{6}\sigma\cos\alpha}{[\sigma/d_{32}]_{\mathrm{w/o}} + [\sigma/d_{32}]_{\mathrm{o/w}}} \tag{4.28}$$

where s represents the surface wetted area per unit volume ($s = 4/D$ for pipe flow), $0 \leq \alpha < 90^o$ corresponds to a surface which is preferentially wetted by water (hydrophilic surface), whereas for $90^o < \alpha \leq 180^o$ the oil is the wetting fluid (hydrophobic surface). The Sauter mean drop size can be scaled with reference to the maximal drop size, $d_{32} = d_{\max}/k_d$. Using such a scaling, models for $d_{\max}$ in coalescing, dense $D_{\mathrm{o/w}}$ or $D_{\mathrm{w/o}}$ can be used in eq. (4.28) to evaluate the critical oil holdup at phase inversion. Applying the H-Model of Brauner (2001), eq. (4.20) yields:

$$\tilde{d}_{\mathrm{o}} = 7.61\tilde{C}_H \left(\frac{\sigma}{\rho_{\mathrm{w}} D U_m^2}\right)^{0.6} \left(\frac{\rho_{\mathrm{w}} U_m D}{\mu_{\mathrm{w}}}\right)^{0.08} \left(\frac{\rho_{\mathrm{w}}}{\rho_m}\right)^{0.4} \frac{\epsilon_{\mathrm{o}}^{0.6}}{(1-\epsilon_{\mathrm{o}})^{0.2}} \tag{4.29}$$

$$\tilde{d}_{\mathrm{w}} = 7.61\tilde{C}_H \left(\frac{\sigma}{\rho_o D U_m^2}\right)^{0.6} \left(\frac{\rho_{\mathrm{o}} U_m D}{\mu_o}\right)^{0.08} \left(\frac{\rho_{\mathrm{o}}}{\rho_m}\right)^{0.4} \frac{(1-\epsilon_o)^{0.6}}{\epsilon_o^{0.2}} \tag{4.30}$$

where d_{o} and d_{w} represent the maximal drop size in $D_{\mathrm{o/w}}$ and $D_{\mathrm{w/o}}$ respectively. Under conditions where the oil-water surface tension in the pre-inversion and post-inversion dispersions is the same (no surfactants or surface contaminants are involved), $(k_d)_{\mathrm{o/w}} \simeq (k_d)_{\mathrm{w/o}}$ and solid-liquid wettability effects can be neglected ($\alpha = 90^o$ or $s \to 0$, as in large diameter pipes, where $d_{\mathrm{o}}, d_{\mathrm{w}} \ll D$), eqs. (4.28 - 4.30) yield:

$$\epsilon_{\mathrm{o}}^I = \frac{\tilde{\rho}\tilde{\nu}^{0.4}}{1 + \tilde{\rho}\tilde{\nu}^{0.4}} \tag{4.31}$$

where $\tilde{\nu}$ is the kinematic viscosity ratio, $\tilde{\nu} = \nu_o/\nu_{\mathrm{w}}$.

Equation (4.31) provides an explanation for the observation made in many experimental studies, that the more viscous phase tends to form the dispersed phase. For a given holdup, and in the case of viscous oil, the characteristic drop size in $D_{\mathrm{o/w}}$ is larger than in the reversed configuration of $D_{\mathrm{w/o}}$. Hence, a larger number of oil drops must be present in order that the surface energy due to the oil-water interfaces would become the same as that obtained with the water dispersed in the oil. Therefore, with $\tilde{\rho}\tilde{\nu}^{0.4} > 1,\ \epsilon_o^I > 0.5,$ and $\epsilon_o^I \to 1$ as $\tilde{\rho}\tilde{\nu}^{0.4} \gg 1$. The larger is the oil viscosity, the wider is

the range of the oil holdup, $0 \leq \epsilon_o < \epsilon_o^I$, where a configuration of oil drops dispersed in water is associated with a lower surface energy. In this range of holdups, the flow pattern will be $D_{\mathrm{o/w}}$ if the operational conditions are in range a the dynamic stability criterion is satisfied. Whereas, $D_{\mathrm{w/o}}$ will be obtained in the range of $\epsilon_o^I \leq \epsilon_o \leq 1$, provided such a dispersion is dynamically stable (see boundaries 4 and 5, Section 5.1). Thus, when only the liquids' interfacial energy is involved, and the hydrodynamic flow field is similar in the initial and post inversion dispersions, the details of the flow field and the system geometry are not required for predicting the critical holdup at inversion.

Figure 4.2 shows a comparison of the critical oil holdup predicted via eq. (4.31), with experimental data of phase inversion in pipe flow which were used by Arirachkaran et al (1989) to obtain their experimental correlation, eq. (4.27) (line 2 in Figure 4.2). A lower variance is however obtained by correlating the data using the form of eq. (4.31). It is worth noting that for high critical oil holdup, corresponding to phase inversion of highly viscous oil dispersions, the water-in-oil dispersion is, in fact, dilute. It was shown by Brauner and Ullmann (2002) that in this range, if d_{w} is modelled by eq. (4.19) (rather than by eq. (4.20)), the critical oil holdup becomes practically independent on the viscosity ratio, in agreement with experimental findings. This phase inversion model was shown

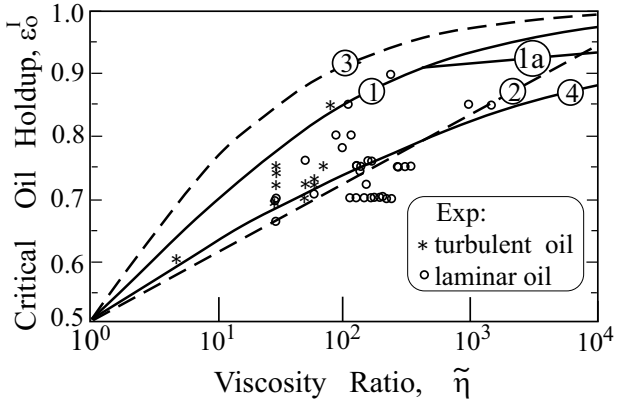

Figure 4.2 The critical oil-cut for phase inversion in pipe- flow - comparison of models/correlations predictions with experimental data: (1)Eq. (4.31); (1a) Eq. (4.28), dilute Dw/o $\mathrm{C_H} = 1$); (2) Eq. (4.27); (3) $\epsilon_o^I = \sqrt{\tilde{\mu}}/(1+\sqrt{\tilde{\mu}})$, (4) Best fit $\epsilon_o^I = \tilde{\mu}^{0.22}/(1+\tilde{\mu}^{0.22})$

to be useful for explaining various experimentally observed features related to phase inversion in pipe flow and in static mixers. These include the effects of the liquids physical properties, liquid/surface wettability (contact angle), the existence of an ambivalent region and the associated hysteresis loop in pure systems and in contaminated systems (Brauner and Ullmann, 2002). Impurities or surfactant, and even entrained air bubbles, may have prominent effect on the critical holdup. Therefore, in many applications it is practically impossible to predict the conditions for phase inversion.

4.6 Conclusion

From the practical point of view, the main issue in predicting the pressure drop in homogeneous liquid-liquid dispersed flow is the modelling of the effective(apparent) mixture viscosity, μ_m. To this aim, the first decision to be made concerns the identity of the continuous phase. This decision is related to the phase inversion phenomenon. The second decision concerns the appropriate model to represent the variation of μ_m with the holdup in the particular system under consideration. The latter depends on the extent of mixing (emulsification) of the dispersed phase, which is a result of a combined effect of many factors (e.g. flow field, liquids physical properties, impurities and/or surfactant, liquid/wall wetting). This factors affect also the critical conditions for phase inversion. In any case, at the phase inversion point the liquids must be at intimate contact and models for emulsion viscosity are applicable to evaluate the pressure drop peak. However, so far, there are no general models or correlations for predicting the effective mixture viscosity for the variety of systems and operational conditions and much empiricism is still involved.

5 Flow Patterns Boundaries

Flow patterns characterization and transitions are usually related to the common parameters, which include the phases flow rates and physical properties. However, in dealing with liquid-liquid systems, the wide ranges of physical properties encountered generate a sort of ambiguity as to how to characterize liquid-liquid systems. It has been shown that it is beneficial to preliminary classify the system according to whether $Eo_D \gg 1$ *or* $Eo_D < 1$ (Brauner, 1998). Large Eotvös (gravity dominated) systems exhibit a similarity to gas-liquid systems, whereby density difference and inclination control flow pattern boundaries. On the other hand, in small Eo_D (surface tension dominated) systems, inclination does not play a role, whereas liquids wettability with the pipe material, entry conditions and start-up procedure are important. In this section some general guidelines for estimating the flow pattern that can be expected under specified operational conditions are outlined.

5.1 Horizontal Systems of $Eo_D >> 1$

Generally, these systems correspond to liquids with a finite density difference and sufficiently large tube diameter. In such systems the stratified flow configuration can be obtained in horizontal and slightly inclined tubes for some range of sufficiently low liquids flow rates. Models suggested for predicting flow patterns transition and guidelines for constructing flow patterns map for such systems are illustrated with reference to Figure (5.1).

1. Transition from (S) to (SM) or (SW) – This boundary defines transition from smooth stratified flow (S) to stratified flow with waves/mixing at the interface, (SW or SM, Figure 1.1b). The transitional criterion evolves from a linear stability analysis carried out on the transient formulation of the two-fluid model, and corresponds to the long-wave

neutral stability boundary. It is given by (Brauner and Moalem Maron, 1993, Brauner, 1996).

$$J_1 + J_2 + J_h = 1 \tag{5.1}$$

$$J_1 = \frac{\rho_1}{\Delta\rho}\ \frac{U_{1s}^2}{Dg\cos\beta}\ \frac{\epsilon_2'}{(1-\epsilon_2)^3}\ \left[\left(\frac{C_{rn}}{U_1}-1\right)^2 + (\gamma_1 - 1)\left(1 - 2\frac{C_{rn}}{U_1}\right)\right] \tag{5.2.1}$$

$$J_2 = \frac{\rho_2}{\Delta\rho}\ \frac{U_{2s}^2}{Dg\cos\beta}\ \frac{\epsilon_2'}{\epsilon_2^3}\ \left[\left(\frac{C_{rn}}{U_2}-1\right)^2 + (\gamma_2 - 1)\left(1 - 2\frac{C_{rn}}{U_2}\right)\right] \tag{5.2.2}$$

$$J_h = C_h\ \frac{\rho}{\Delta\rho}\ \frac{(U_1-U_2)^2}{Dg\cos\beta}\ \frac{4S_i}{\pi\epsilon_2(1-\epsilon_2)D}\ ; \tag{5.2.3}$$

where:

$$C_{rn} = \frac{\frac{U_2}{\epsilon_2}\ \frac{\partial\Delta F_{12}}{\partial U_2} - \frac{U_1}{(1-\epsilon_2)}\ \frac{\partial\Delta F_{12}}{\partial U_1} - \frac{\partial\Delta F_{12}}{\partial\epsilon_2}}{\left[\frac{1}{\epsilon_2}\ \frac{\partial\Delta F_{12}}{\partial U_2} - \frac{1}{(1-\epsilon_2)}\frac{\partial\Delta F_{12}}{\partial U_1}\right]}\ ;\ \epsilon_2 = \frac{A_2}{A}\ ;\ \epsilon_2' = \frac{d\epsilon_2}{d(h/D)} \tag{5.2.4}$$

$$\Delta F_{12} = \frac{\tau_2 S_2}{A_2} - \tau_i S_i\left(\frac{1}{A_2} + \frac{1}{A_1}\right) - \tau_1\frac{S_1}{A_1} + (\rho_2 - \rho_1)\, g\sin\beta \tag{5.2.5}$$

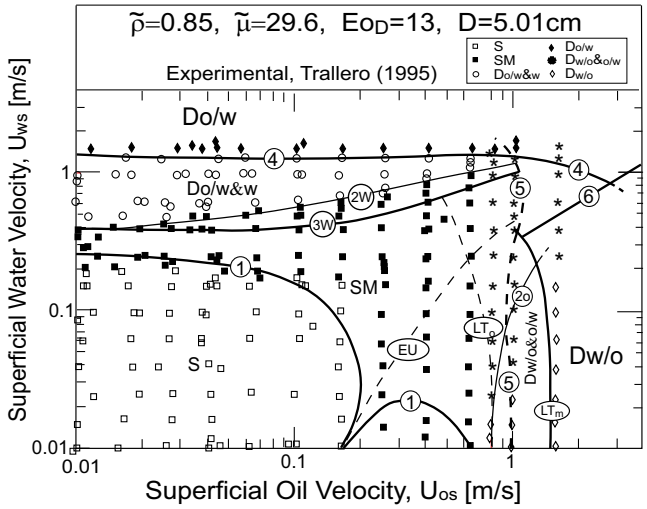

Figure 5.1 The construction of a flow pattern map for horizontal oil-water flow, $Eo_D \gg 1$ comparison of models prediction Trallero (1995) data.

All flow variables in eqs. (5.2) (phases velocities U_1, U_2, wall shear stresses τ_1, τ_2, τ_i flow cross-sectional area A_1, A_2 and wetted perimeters S_1, S_2, S_i) are those obtained for

steady smooth stratified flow corresponding to superficial phases velocities U_{1s}, U_{2s} (see Section 2.4 and Figure 2.1). For $Eo_D \gg 1$, a plane interface can be assumed ($\phi^* = \pi$), whereby the flow geometry is determined by the lower layer depth, h. The shape factors γ_1, γ_2 (assumed constant) account for the velocity profiles in the two layers. For plug flow $\gamma_1 = \gamma_2 = 1$ and $\gamma > 1$ corresponds to a layer with a significant velocity gradient. Equation (5.1) represents a generalized stability criterion, which includes the Kelvin-Helmholtz mechanism and 'wave sheltering' mechanism. The destabilizing terms are due to the inertia of the two liquids (J_1, J_2 terms) and due to the dynamic interaction of the growing waves with turbulence in the faster layer, J_h. For laminar stratified layers $J_h = 0$. Otherwise a correlation for C_h is needed, but it is available only for gas-liquid systems. In liquid-liquid systems, the J_h term may be less significant (since the velocity difference is much smaller), and the stability criteria has been applied assuming $J_h = 0$ (Brauner and Moalem Maron, 1992a, 1992b).

Criterion (5.1) defines the combinations of U_{1s} and U_{2s} which corresponds to the evolution of interfacial disturbances (SW) and thus, possible entrainment of drops at the liquids layer interface (SM). This boundary is denoted by 1 in Figures 5.1 and 5.2, and is shown to predict the conditions for the evolution of interfacial disturbances in horizontal and inclined flows. Note that, in these Figures, the oil and water correspond to the lighter and heavier layer, respectively, $U_{1s} \equiv U_{os}$ and $U_{2s} \equiv U_{\rm ws}$.

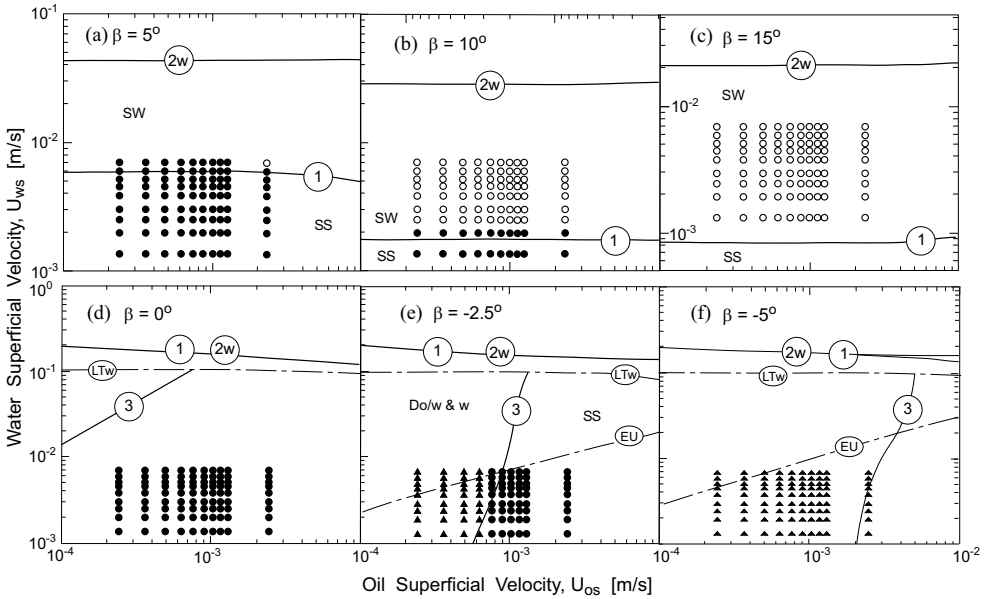

Figure 5.2 Effect of tube inclination on the SS boundaries. Experiment • SS ∘ SW ▲ elongated oil drops (Gat, 2002).

2. Upper bounds on patterns involving stratification – Outside the region of stable (smooth) stratified flow (boundary 1) the flow pattern is stratified wavy flow with drop entrainment at the interface. The rate of droplet entrainment increases with increasing the liquids flow rates and various flow patterns which still involve stratification may develop (see Figures

1.1c to 1.1h). The stratified flow configurations are confined to a domain at whose boundaries the two-fluid formulation (for stratified configuration) becomes ill-posed (Brauner and Moalem Maron, 1991,1992d Brauner, 1996). The condition for ill-posedness is given by:

$$\widetilde{\rho}_2 U_2^2 \gamma_2(\gamma_2 - 1) + \widetilde{\rho}_1 U_1^2 \gamma_1(\gamma_1 - 1) - (\gamma_2 U_2 - \gamma_1 U_1)^2 + \\ + \frac{D}{\rho_{12}}[(\rho_2 - \rho_1) g \cos\beta - C_h \rho (U_1 - U_2)^2 S_i (A_1^{-1} + A_2^{-1})] \leq 0 \tag{5.3}$$

where $\widetilde{\rho}_2 = 1 + \frac{\rho_2}{\rho_1}\frac{A_1}{A_2}$, $\widetilde{\rho}_1 = 1 + \frac{\rho_1}{\rho_2}\frac{A_2}{A_1}$, $\rho_{12} = \frac{D(dA_2/dh)\rho_1\rho_2}{A_2[\rho_1 + \rho_2 A_1/A_2]}$. The ill-posedness boundary is indicated in Figure 5.1 by the two branches, 2w for a faster lower water layer and 2o for a faster upper oil layer. As shown in the figure, the ill-posedness boundary is always located in the region of amplified interfacial disturbances since the stable smooth stratified zone, which is confined by the stability boundary 1, is always a sub-zone of the well-posed region. Boundary 2w in Figure 5.1 was obtained with $\gamma_1 = 1.1$ for low U_{1s}, which was gradually reduced to $\gamma_1 = 1$ for higher oil rates where both layers are turbulent and $U_1 \simeq U_2$.

As shown in Figure 5.1 boundary 2w marks the location of SM to Do/w&w transition. The auxiliary lines, which provide useful information on the flow pattern that can be expected are the locus of $h/D = 0.5$; the locus of laminar/turbulent transition in the lower (water) layer LTw, laminar/turbulent transition in the oil layer, LTo (evolution of enhanced dispersive forces in either the water or oil layer) and the locus of $U_o = U_{\rm w}$, EU. Figure 5.1 points out an important difference between liquid-liquid systems and gas-liquid systems. In oil-water systems, the densities of the fluids are similar and therefore, the line of equal layers' velocity divide the zone of stable stratification into two regions, either faster oil layer or faster water layer. Entrainment of oil drops into the water layer takes place when $U_{\rm w} > U_o$ (left to the equal velocity curve, EU), whereas entrainment of water drops into the oil layer is associated with $U_o > U_{\rm w}$ (right to the EU curve). The dispersion of water drops into the oil layer is enhanced by transition to turbulent oil layer. However, as long as the water and oil flow rates are within the region where the transient stratified flow equations are well-posed (below curve 2w and below curve 2o), the flow patterns may involve a certain stratification, where in the upper layer, the oil forms the continuous phase and in the lower layer water is the continuous phase. It is worth noting that in contrast to gas-liquid systems, the entrained drops (water into oil, or oil into water) do not posses sufficient momentum to penetrate through the dense continuous phase and impinge on the tube walls. Therefore, the onset of drops entrainment in liquid-liquid systems is usually *not* associated with the formation of liquid film on the tube surface and the consequential transition to annular flow.

3w. Transition to Do/w&w – For $U_{\rm w} \gg U_o$ and outside boundary 1, the fragmentation of oil drops from the wavy oil-water interface is due to the inertia forces exerted by the faster water flow and is represented by the eq. (4.25) with $\Delta U_c = U_{\rm w} - U_o$. A dispersion of the entrained oil drops is stable provided $d_{\max} < d_{crit}$. The critical drop size, d_{crit} is taken as:

$$\frac{d_{crit}}{D} = Min\left(\frac{d_{c\sigma}}{D}\ ,\ \frac{d_{cb}}{D}\right) \tag{5.4}$$

where $d_{c\sigma}$ represents the maximal size of drop diameter above which drops are deformed (Broodky, 1969):

$$\tilde{d}_{c\sigma} = \frac{d_{c\sigma}}{D} = \left[\frac{0.4\sigma}{\mid \rho_c - \rho_d \mid g\cos\beta' D^2}\right]^{1/2} = \frac{0.224}{(\cos\beta')^{1/2} Eo_D^{1/2}} \tag{5.5.1}$$

$$Eo_D = \frac{\Delta\rho g D^2}{8\sigma} \quad ; \quad \beta' = \begin{cases} \mid \beta \mid & ; \quad \mid \beta \mid < 45^o \\ 90 - \mid \beta \mid & ; \quad \mid \beta \mid > 45^o \end{cases} \tag{5.5.2}$$

and d_{cb} is the maximal size of drop diameter above which buoyant forces overcome turbulent dispersive forces in the continuous phase and therefore, migration of the drops towards the tube walls takes place (Barnea, 1987):

$$\tilde{d}_{cb} = \frac{d_{cb}}{D} = \frac{3}{8}\frac{\rho_c}{\mid \Delta\rho \mid}\frac{f U_c^2}{Dg\cos\beta} = \frac{3}{8} f \frac{\rho_c}{\Delta\rho g} Fr_c \; ; \qquad Fr_c = \frac{U_c^2}{Dg\cos\beta} \tag{5.6}$$

with β denoting the inclination angle to the horizontal (positive for downward inclination). Equation (5.6) is relevant only in shallow inclinations and in case of turbulent flow in the faster (water) layer ($U_c \equiv U_{\rm w}$). Moreover, in oil-water systems, where $\Delta\rho/\rho_c \ll 1, \widetilde{d}_{cb} > \widetilde{d}_{c\sigma}$, and in most practical cases $\widetilde{d}_{crit} = \widetilde{d}_{c\sigma}$ is used. In this case, the following transitional criterion evolves from eqs.(4.25) and (5.5.1) (Brauner, 2000):

$$\Delta U_c \equiv U_{\rm w} - U_o \geq 4.36 \left[\frac{\sigma\Delta\rho g\cos\beta'}{\rho_c^2}\right]^{1/4} \left\{1 + 1.443\left(N_{vd}\cos\beta'\right)^{0.4}\right\}^{1/2} \tag{5.7}$$

where N_{vd} is the viscosity number of the dispersed oil phase, $N_{vd} = \frac{\mu_d^4 \Delta\rho g}{\rho_d^2 \sigma^3}$, $\mu_d \equiv \mu_o, \rho_d \equiv \rho_o, \rho_c \equiv \rho_{\rm w}$. The constant coefficient (4.36) in eq. (5.7) may require some tuning when applied to a specific two-fluid system. According to this model, drops entrainment takes place when the velocity gap between the continuous (water) layer and the layer which is being dispersed (oil) exceeds a threshold value. This threshold value is given by the r.h.s. of eq.(5.7) and is independent of the tube diameter. For instance, a typical low viscosity oil-water system would be $\rho_c \simeq 1 gr/cm^3$ $\Delta\rho = 0.1\rho_c$ and $\sigma = 30 dyne/cm$, which yields a velocity gap of $0.3 m/s$ that is required for significant entrainment. Boundary 3w in Figure 5.1 corresponds to eq. (5.7). It is worth noting that this figure is typical to low viscosity oil. For highly viscous oils ($\mu_0 > 1$ poise), the threshold value for the onset entrainment of oil drops into water increases (due to $N_{vd} >> 1$) in eq. (5.7). Also, the line of equal velocities of the oil and water layers is shifted to higher oil flow rates. Consequently, the zone outside the neutral stability boundary (up to boundary 2w may partially (or entirely) correspond to wavy stratified flow (SW), rather to stratified mixed flow (SM).

In systems which are not absolutely dominated by gravity ($Eo_D \simeq 1$), the Do/w&w pattern can be obtained instead of a continuous oil layer even for a small velocity gap. This can happen with a hydrophilic tube surface and when the largest oil drop that can occupy the upper part of the tube is smaller than the critical drop size. The criterion suggested for this transition (Brauner and Moalem Maron, 1992b,1992c):

$$A_1 \cos\beta \leq \pi d_{crit}^2/4 \quad ; \quad d_{crit} = C\left[\frac{\sigma}{\Delta\rho g}\right]^{1/2} \tag{5.8}$$

provided the resulting $U_{1s}(\equiv U_{os})$ and $U_{2s}(\equiv U_{\rm ws})$ are within the regions of stable stratification (below boundary 2w). While this criterion is irrelevant for predicting the flow patterns data in Figures 5.1, it is shown to predict the appearance of Do/w&w at low water and oil flow rates in upward inclined tubes (Figure 5.2e,f) and the gradual vanishing of the stratified flow pattern with increasing the upward inclination.

3o. Transition to Do/w&w – For $U_o \gg U_{\rm w}$ and outside boundary 1, eq.(4.25), and thus eq.(5.7), is applied with $\Delta U_c = U_o - U_{\rm w}, \mu_d \equiv \mu_{\rm w}, \rho_d \equiv \rho_{\rm w}$ and $\rho_c \equiv \rho_o$. This yields the critical velocity gap for dispersing the water layer into the oil layer. For the system studied in Figure 5.1, boundary 3o (not shown) is similar to 2o.

In systems of $Eo_D = O\{1\}$ and hydrophobic tube surface, eq. (5.8) with A_2 replacing A_1 signals transition to Dw/o&o due to capillary effects.

4. Transition to Do/w – A homogeneous oil-in-water dispersion (emulsion) can be maintained when the turbulence level in the continuous water phase is sufficiently high to disperse the oil phase into small and stable spherical droplets of $d_{\max} < d_{crit}$. Applying this criterion using the extended Hinze model, eqs. (4.18 to 4.21) with eqs. (5.4 to 5.6), yields a complete transitional criteria to dispersed flows (H-Model, Brauner, 2001). When the fluids flow rates are sufficiently high to maintain a turbulence level where $d_{\max} < d_{c\sigma}$ and $d_{\max} < d_{cb}$, spherical nondeformable drops are formed and the creaming of the dispersed droplets at the upper or lower tube wall is avoided. Thus, the fully dispersed flow pattern can be considered as stable. In these equations $U_c = U_m, U_{cs} = U_{\rm ws}, U_{ds} = U_{os}, \rho_c = \rho_{\rm w}$ and $\mu_c = \mu_{\rm w}$. Hence, $We_c = \frac{\rho_{\rm w} D U_m^2}{\sigma}$; $Re_c = \frac{DU_m}{\nu_{\rm w}}$ and $\epsilon_d = U_{os}/U_m$. For instance, if $d_{crit} = d_{c\sigma}$, the transitional criterion reads:

$$C_{(\epsilon_d)} Eo_D^{1/2} We_c^{0.6} Re_c^{0.08} \geq 1 \tag{5.9}$$

The variation, $C_{(\epsilon_d)}$ with the dispersed phase holdup evolves from the H-model equations.

Curve 4 in Figure 5.1 predicts the transitional boundary from Do/w&w to Do/w. In systems of $Eo_D \simeq 1$, the K-model (eqs. 4.23 and 4.24) replaces the H-model in the evaluation of $d_{\max}$ (Brauner, 2001).

5. *Transition to* Dw/o – A homogeneous water-in-oil dispersion (emulsion) develops when turbulence level in the continuous oil phase is sufficiently high to disperse the water phase into stable small droplets. In this case eqs.(4.18 to 4.20) and (5.4 to 5.6) are applied with $U_c = U_m, U_{cs} = U_{os}, U_{ds} = U_{\rm ws}, \rho_c = \rho_o$ and $\mu_c = \mu_o$. Hence, $\epsilon_d = U_{\rm ws}/U_m$ and $We_c = \frac{\rho_o D U_m^2}{\sigma}$; $Re_c = \frac{DU_m}{\nu_o}$. In systems of $Eo_D \simeq 1$, eqs. (4.23 - 4.24) replace eqs. (4.19 - 4.20) for the evaluation of $\widetilde{d}_{\max}$. Boundary 5 in Figure 5.1 corresponds to the predicted transition to Dw/o. It is worth noting that for the critical flow rates along boundary 4, the mixture Reynolds number is already sufficiently high to assure turbulent flow in the water. However, when a viscous oil forms the continuous phase, the locus of the transition to $D_{\rm w/o}$ may be constrained by the minimal flow rates required for transition to turbulent flow in the oil ($Re_c = 2100$ along boundary LT_m). The required turbulent dispersive forces exist only beyond the LT_m boundary, which therefore forms a part of the $D_{\rm w/o}$ transitional boundary.

6. Transition from Do/w to Dw/o - This transition is associated with the phase inversion phenomena discussed in Section 4.5. Boundary 6 in Figure 5.1 was obtained by eq. (4.31). The phase inversion model is applicable for predicting this transition when the oil and water flow rates are sufficiently high to sustain both a homogeneous Do/w and Dw/o. As shown in Figure 5.1, boundaries 4 and 5 indeed define an ambivalent range where either of the oil or water phase can be homogeneously dispersed. It is the phase inversion phenomenon which eventually defines the boundaries of Do/w and Dw/o.

7. Core flow boundaries – In highly viscous oils, the laminar regime extends to high oil flow rates. In the absence of turbulent dispersive forces in the oil phase, it is possible to stabilize a viscous oil core which is lubricated by water annulus. The region were stable CAF is feasible is: (a) outside the boundaries of stable stratification (outside 2w and 2o), hence, sufficiently high oil rate (and water cut) to overcome the float-up tendency of the lighter oil core; (b) in the CAF configuration, the difference between the velocity of the oil in the core ($U_c \equiv U_o$) and the water velocity in the annulus ($U_a \equiv U_{\rm w}$), should not exceed the threshold value which would result in entrainment of the water film into the oil core. The threshold value is given by the r.h.s. of eq. (5.7), with $\rho_c = \rho_o$ ($N_{vd} = \mu_{\rm w}^4 \Delta\rho g/\rho_{\rm w}^2\sigma^3 \ll 1$ and can be ignored). The core annular model in section 3.2 can be used to evaluate U_c and U_a. However, since for turbulent water film, the slip between the phases is only few percents of the core velocity, this condition constrains the CAF only at high U_{os}; (c) water cut should not exceed a threshold value which results in disintegration of the oil core into oil globes by a thick wavy water annulus. Favorable conditions for wave bridging are $A_a/A_c > 1$. Using the annular flow model (Section 3.2) yields the flowing criterion for avoiding transition from core flow to oil slugs:

$$\frac{U_{os}}{U_{\rm ws}} \equiv \frac{U_{cs}}{U_{as}} \geq \frac{\mu_a}{\mu_c} + 2 \; ; \qquad \text{laminar core-laminar annulus} \qquad (5.10)$$

$$\frac{U_{cs}}{U_{as}} \geq 2.875 \times 10^{-3} \frac{\mu_a}{\mu_c} Re_{as}^{0.8} + 1.15 \; ; \qquad \text{laminar core-turbulent annulus}$$

These criteria were shown to provide reasonable estimations of the oil and water flow rates where core flow is stable (see Figures 19 and 20 in Brauner,1998). The minimal water-cut needed to avoid stratification decreases with increasing the the oil core viscosity.

It is worth emphasizing the evolution of annular flow due to pure dynamical effects in systems of $Eo_D \gg 1$ (as in gas-liquid horizontal flows) is unlikely for oils of relatively low viscosity. Stabilization of the core requires sufficiently high velocity of the core phase: high mixture velocity and high input cut of the core phase. Under such conditions (and with low oil viscosity), dispersive forces are dominant and emulsification of the potential annular phase into the core phase results in a fully dispersed (emulsion) of the annular liquid within the core liquid and destruction of the CAF configuration.

5.2 Systems of $\mathbf{Eo_D \ll 1}$

Such systems exhibit flow patterns which are similar to microgravity systems (Brauner, 1990). The tube diameter is smaller than d_{crit} and in view of criterion (5.8) stratified

flow will not be obtained even for low oil and water rates. The drift velocity of drops is negligible and the tube inclination has no effect on the flow patterns. Also, different flow patterns may result by changing the liquids/wall wettability properties (changing the tube material or the start-up procedure).

In hydrophilic tube, for low oil flow rate and high water cut, the flow pattern is oil droplets dispersed in water. With increasing the oil rate, enhanced droplets coalescence yields larger spherical oil drops (bubbles) with $d \simeq D$. This transition usually occurs for in situ oil holdup of about $0.15 \div 0.25$ corresponding to $\widetilde{Q}^{-1} = \frac{U_{\rm ws}}{U_{os}} = \frac{\epsilon_o}{1-\epsilon_o} = \simeq 0.17 \div 0.33$. For larger oil in situ holdup, the large spherical bubbles coalesce to form elongated oil bubbles (oil slugs). This transition takes place when the oil in situ holdup approaches the maximal volumetric packing, $\epsilon_o \simeq 0.4 \div 0.5$ corresponding to $\widetilde{Q} \simeq 1 \div 1.5$.

The slug/annular transition takes place for sufficiently low water cut, where stable thin water annulus can be maintained. This boundary can be calculated by eq. (5.10). For low viscosity oil and high oil rates, the oil core is turbulent. When the turbulent dispersive forces are sufficiently high to disperse the water annulus, transition to Dw/o takes place. It should be noted that in systems of $Eo_D \ll 1$, $d_{crit} = d_{c\sigma} > D$. Therefore, d_{crit} is scaled by D (e.g., $d_{crit} \simeq D/2$,and the K1-model in Brauner, 2001 is used to calculate the transition to Dw/o (boundary 5), or Do/w (boundary 4)). The entrainment of the water film due to the inertia of the core phase should also be considered. The corresponding critical velocity difference is given by eq. (5.7), with $\Delta U_c = U_o - U_{\rm w} = U_c - U_a$ (using the CAF model in section 3.2 to calculate the velocity difference). The locus of Do/w to Dw/o transition at high oil and water rates is obtained by the phase inversion model (eq. 4.28). The application of these criteria for predicting flow pattern transition in systems of low Eo_D was demonstrated in Brauner,1998.

In a hydrophobic tube, there is evidence that for low oil water rates and high water cut inverted annular flow (Andreini, et al., 1997) with oil flowing in the annulus can be obtained (instead of Do/w). This flow pattern can be maintained as long as the level turbulence in the water core, as well as its inertia, are not sufficiently high to disperse the oil annulus. Also, the oil holdup in the annulus must be sufficiently low to avoid blockage of the water core ($A_c/A_a \geq 1$, A_c, A_a calculated via the annular flow model, Section 3.2).

5.3 Vertical upward systems

The construction of a flow pattern map for vertical upward oil-water flows is demonstrated in Figures 5.3 and 5.4. The basic flow configuration for low superficial oil velocity is Do/w. For low water rates, the oil is dispersed in the water in the form of relatively large bubbles. The criterion of $\epsilon_o \geq 0.25$ is usually suggested to mark transition from small spherical bubbles to large oil bubbles and slugs (e.g., Harsan and Kabir, 1990). The locus of $\epsilon_o = 0.25$ (as predicted via eq. (4.5) and (4.6)) is indicated by boundary 8. With increasing the water rate, transition to fine Do/w (o/w emulsion) takes place, which is predicted by transition 4. Similarly, the transition to fine Dw/o (w/o emulsion) takes place for sufficiently high oil superficial velocities (transition 5) which are higher than that required for establishing turbulent flow in the oil as a continuous phase (right to boundary LT_m). The phase inversion model yields the boundary between Do/w and Dw/o (transition 6).

The unstable region of churn flow is obtained for low water rates and intermediate oil rates. The oil flow rate is too high to sustain a stable configuration of Do/w. Large oil bubbles (of the order of $d \simeq d_{crit}$) coalesce and tend to form an oil core surrounded by a water annulus (CAF). Boundary 7 in Figure 5.3 is the locus of $\widetilde{D}_c = 0.5$ as predicted by the CAF model for vertical upward flow (a thinner core results in transition to oil bubbles dispersed in water). However, the oil velocity is too low to meet the dynamic requirements for stabilization of oil dominated flow patterns, namely, oil forms the continuous phase as in CAF flow or Dw/o. For stable CAF, the oil superficial velocity should be sufficiently high to suspend large water drops, $d \simeq D$ (say $d = D/2$), which are occasionally formed, whereby:

$$\frac{1}{8}\pi d^2 C_D \rho_o U_{os}^2 \geq \frac{1}{6}\pi d^3 (\rho_{\rm w} - \rho_o) \;\; ; \;\; \text{or} \;\; U_{os}\left[\frac{\rho_o}{\Delta\rho g D}\right]^{1/2} \geq \left(\frac{2}{3C_D}\right)^{1/2} \tag{5.11}$$

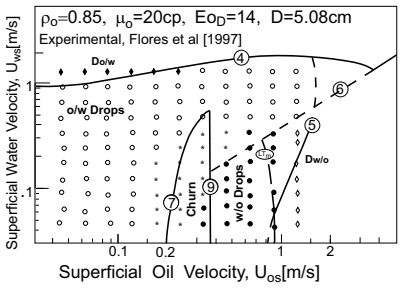

Figure 5.3 The construction of a flow pattern map for vertical oil-water system-comparison with Flores et al, (1997) data.

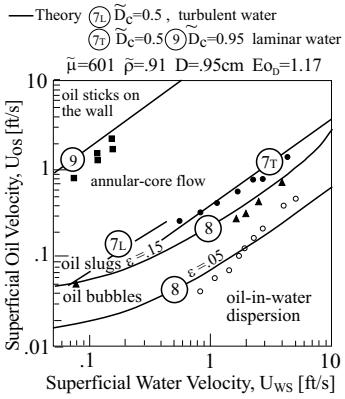

Figure 5.4 Flow pattern map for vertical upward flow of water and highly viscous oil (μ_0=601 cp)-comparison with Bai et al, (1992) data.

Boundary 9 in Figure 5.3 has been obtained by eq. (5.11) with $C_D = 0.44$. It is worth noting that criterion (5.11) is similar to that of flow reversal of the annular film, which is frequently used to estimate flooding conditions, as well as transition to annular flow in upward gas-liquid systems. Condition (5.11), however, introduces the effect of the oil viscosity (and drop size) through the variation of C_D. It is worth emphasizing that with relatively low viscosity oils (as is the case in Figure 5.3) the CAF configuration is eventually not obtained. The potential water annulus is dispersed into the oil phase to form the Dw/o pattern. The annular pattern in upward vertical flow has been observed only for highly viscous oils. The size of oil bubbles and slugs increases with the oil viscosity and for sufficiently large oil-cut, a continuous oil core surrounded by a water film may be formed (see Figure 5.4). Oil core flow lubricated by a water annulus was obtained for sufficiently high oil cut (instead of the churn regime observed with low viscosity oils). The core interface is wavy and water rate should be kept higher than a threshold value to prevent oil sticking on the tubes wall. Indeed, with highly viscous oils

($Re_d = \rho_o U_{os} d/\mu_o \ll 1$ and $C_D = 24/Re_d$) condition (5.11) is satisfied already for low oil velocities and the region of churn flow in Figure 5.3 is occupied by the CAF in Figure 5.4. As shown, the core flow region in Figure 5.4 can be estimated using the CAF model (Section 3.2) for calculation the core phase holdup. It extends from $\tilde{D}_c \simeq 0.5$ (transition to slug flow) to $\tilde{D}_c = 0.95$ (oil sticks to the wall).

5.4 Conclusion

The first step in the construction of a flow pattern map for a liquid liquid system is its classification according to its Eotvös number, to either being gravity dominated or surface tension dominated system. The guidelines and criteria for flow pattern transitions as outlined above, were found useful for estimating the flow pattern map for these two types of liquid liquid systems. However, these have still to be tested in view of more data in the variety of liquid-liquid systems, pipe diameters, materials and inclinations.

Table 1.1.1 Summery of Experimental Systems of Liquid -Liquid Horizontal Flow

Authors	D [cm] pipe material	μ_o/μ_w	ρ_o/ρ_w	σ dyne/cm	Additional Measurements	Observed Flow Patterns
Russell *et al.* (1959)	2.03 Cellulose Acetate-Butyrate	20.13	0.840		dP/dl ε_w	SM, Do/w, Bo
Charles *et al* (1961)	2.64 Cellulose Acetate-Butyrate	6.29 16.8 65	1 1 1	44 45 30	dP/dl ε_w	Do/w, ANw, SLo, Bo
Guzhov *et al.* (1973)	3.94 Steel	21.8	0.898	44.8	dP/dl	SM, Dw/o, Do/w Do/w & w, Dw/o & o/w
Malinowsky (1975)	3.84 Steel	3.33	0.850	22.3	dP/dl	SM, Do/w, Dw/o Dw/o & o/w
Laflin & Oglesby (1976)	3.84 Steel	4.12	0.830	22.3	dP/dl	SM, Do/w, Dw/o Dw/o & o/w
Oglesby (1979)	4.1 Steel	32 61 167	0.859 0.863 0.870	30.1 29.4 35.4	dP/dl	Do/w, Dw/o Dw/o & o/w
Cox (1985)	5.08 Acrylic	1.54	0.756		ε_w	S, Do/w Do/w & w
Scott (1985)	5.08 Acrylic	1.54	0.756		ε_w	S, o/w Do/w & w
Stapelberg & Mewes (1990)	2.38 5.9 Acrylic ,glass	30	0.852	50	dP/dl	SM, Do/w & w Dw/o & o/w
Fujii *et al* (1994)	2.5 Acrylic	61.5	0.98	29	dp/dl ε_w	Bo, Bw, SLo, SLw, ANo
Valle & Kvandal (1995)	3.75 Glass	2.55	0.792	37.3	dP/dl, ε_w (Conductivity & sampling probes)	S, SM Do/w & w Dw/o & o/w
Trallero (1995)	5.08 Acrylic	29.7	0.852	36	dP/dl ε_w	S, SM Do/w & w Do/w,Dw/o Dw/o & o/w Dw/o & w
Nadler & Mewes (1997)	5.9 Perspex	18-35	0.848		dP/dl Phase continuity (Conductivity probe)	S, SM Do/w & w Do/w, Dw/o Dw/o & o/w Dw/o & w
Vedapuri *et al.* (1997)	10.12 Plexi-glass	2			ε_w isokinetic probe	SM, Dw/o & o/w
Beretta *et al* (1997)	0.3 Borosilicate glass	9.9, 51.3, 71.2	0.87, 0.89, 0.87	37.4, 36, 31.5	dp/dl	Do/w, SLo, Bo, ANw

Table 1.1.1 *Continued*

Kurban *et al* (1997)	2.43, 2.4 St. steel Acrylic	1.6	0.803	17	dP/dl (Conductivity & Impedance probe)	S, SM, Dw/o
Andreini *et al* (1997)	0.3, 0.6 Borosilicate glass, Steel, Copper, PVC	562, 920, 1307	0.886, 0.889, 0.893		dp/dl	Do/w, SLo, PLo, ANw
Valle & Utvik (1997)	7.62 Steel	1	0.741		dp/dl (Conductivity probe)	Do/w , Dw/o, S
Hapanowicz *et al* (1997)	1.2 1.6 2.2 Glass	40 40	1.2 0.915			Do/w, Dw/o, Dw/o&o, Do/w&w, Dw/o&w, S, DANo, PL, Foam
Angeli & Hewitt (1998)	2.43, 2.4 St. steel Acrylic	1.6	0.803	17	dP/dl (Conductivity and Impedance probe)	S, Do/w, Dw/o, Do/w &w, Dw/o &o, Dw/o &o/w
Soleimani (1999)	2.43 St. steel	1.6	0.803		dP/dl, ε_w Phase distribution (High Frequency Impedance probe & Gamma Densiometer)	SM, Dw/o &o/w
Angeli & Hewitt (2000)	2.43, 2.4 St. steel Acrylic	1.6	0.803	17	ε_w (Conductivity and Impedance probe)	S, Do/w, Dw/o, Do/w &w, Dw/o &o, Dw/o &o/w
Lovick *et al.* (2000)	3.8 Stainless Steel	5.25	0.828	44.7	dP/dl, ε_w (conductivity probe)	S, SM Do/w, Dw/o
Fairuzov *et al* (2000)	36.35 Steel	5.07	0.853		Volume fraction (Multi-Point Sampling Probe)	S Do/w & w
Simmons & Azzopardi (2001)	6.3 PVC	1.125	0.684	10	Drop size, velocity & distribution (Par-Tec 300C, Malvern 2600)	SM, Dw/o & w, Dw/o
Angeli *et al.* (2002)	3.8 Stainless Steel	5.25	0.828	44.7	dP/dl Phase distribution (Impedance probe, conductivity probe)	SW, Do/w, Dw/o &o/w, Dw/o

Table 1.1.2 Summery of Experimental Systems of Liquid -Liquid Core Annular Flow

Authors	D [cm] pipe material	Core Fluid	Annulus Fluid	μ_o/μ_w	ρ_o/ρ_w	σ dyne/cm	Additional Measurements
Charles *et al* (1961)	2.64 Cellulose Acetate-Butyrate	20.6% CTC in Marcol GX 18.7% CTC in Wyrol J 16.7% CTC in Teresso 85	Water Water Water	6.3 16.8 65	1 1 1	44 45 30	dP/dl
Kruyer *et al* (1967)	1.35, 3.19, 10.24 Copper, Acrylic, Steel, Aluminum	lubricating oil	Water	36, 28, 6, 17	0.86 0.86 0.83 0.85		dP/dl
Sinclair (1970)	1.905, 2.54, 6.35	Humble Fractol oil, water, emulsifier	Sea Water	1000	0.94		
Hasson & Nir (1970)	1.26 Glass	water	Kerosene-Perchloroethylene	1.2	1.02	17-17.5	film thickness
Hasson *et al* (1970)	1.26 Glass	water	Kerosene-Perchloroethylene	1.2	1.02	17-17.5	breakup mechanism
Hasson (1978)	0.9 Stainless Steel	water	Kerosene	1.6	0.803	17	Heat transfer & coefficients, scaling
Wu *et al* (1986)	5.08 Transparent	Zuata crude oil	water	2200, 10000	0.992 ,0.997		dp/dl specific energy consumption
Oliemans (1986)	5.08, 20.32 Perspex	oil	water	2584	0.97		dp/dl ε_w Wave characteristic
Guevara *et al* (1988)	20.3 Stainless Steel	viscous hydrocarbon	water	up to 110,000	0.995		dp/dl water fraction
Anon (1988)	20.27 Stainless Steel	Zuata crude oil	water	3,000 - 100,000			dp/dl water fraction
Bai *et al* (1992)	0.9525 Glass	oil	0.4% Sodium Silicate in Water	601	0.906	8.54	dp/dl ε_w
Miesen *et al* (1992)	5.08, 20.32	fuel crude	water water	13-25 30-42	0.96-0.97 0.98-0.99	20-50	dp/dl Wave characteristic
Arney *et al* (1993)	1.59 Glass	waxy crude oil No. 6 fuel oil	water water	600 2700	0.985 0.989	-- 26.3	dp/dl ε_w
Ho & Li (1994)	1.9, 7.3	10%v/v ECA polyamine surfactant in diesel	2%w/w KCl in water	109,091	0.836		dp/dl Annular size
Andreini *et al* (1997)	0.3, 0.6 Borosilicate glass, Steel, Copper, PVC	Miplar	water	562, 920, 1307	0.886, 0.889, 0.893		dp/dl

Table 1.2 Summery of Experimental Systems of Liquid -Liquid Inclined Flow

Authors	β(°)	D [cm] pipe material	μ_o/μ_w	ρ_o/ρ_w	σ dyne/cm	Additional Measurements	Observed Flow Patterns
Soot & Knudsen (1972)	-90	1.89 Brass	0.98 8.6 180		40 -- 13	dp/dl ε_w	Do/w
Mukhopadhyay (1977)	±30 to ±90	3.81 Lexan	5-6	0.850		dP/dl ε_w	
Mukherjee *et al* (1981)	±30 to ±90	3.81 Lexan	5-6	0.852	22.3	dP/dl ε_w	Do/w & w/o
Hill & Oolman (1981)	+30 to +90	15.2, 21.6, 11.4 Steel, Acrylic	1.6	0.801	17	dP/dl ε_w	Bo, S
Cox (1985)	-15,-30	5.08 Plexiglass	1.54	0.756		ε_w	S, Do/w Do/w & w
Scott (1985)	+15,+30	5.08 Plexiglass	1.54	0.756		ε_w	S, Do/w Do/w & w
Vigneaux *et al* (1988)	+25 to +90	20		0.741		Phase distribution (Impedance probe)	Do/w
Zavareh *et al* (1988)	+85 and +75	18.41 Acrylic	2.46	0.783			Bo, dispersed bubbly
Tabeling *et al* (1991)	+15 to +90	20	5	0.782			
Ding *et al* (1994)	+30, +45, +60, +90	16.51 Transparent		0.811		ε_w	
Kurban (1997)	1+	7.79 Stainless Steel	45	0.865			S, SM, Do/w & w, Dw/o & o
Vedapuri *et al* (1997)	±2	10.16 Acrylic	2,96			ε_w	Semi-segragated Semi-dispersed
Flores (1997)	45,60,75,90	5.08 Acrylic	20	0.858	33.5	dP/dl ε_w (conductivity probe)	Do/w CT, Do/w PS, VFDo/w Dw/o CC, VFDw/o, Churn TF
Hassan & Kabir (1999)	+45, +75, +85	6.24, 12.7 Plexiglass	1.6	0.801	17	ε_w	Bo, Bw, SLo, SLw
Alkaya *et al* (2000)	0,±0.5,±1, ±2,±5	5.08 Acrylic	18	0.854	36	dP/dl ε_w	S, SM
Angeli *et al.* (2002)	0, +5	3.8 Stainless Steel	5.25	0.828	44.7	dP/dl Phase distribution (Impedance probe, conductivity probe)	S, Do/w, Dw/o, Do/w &w/o
Gat (2002)	0 - ±30	1.44 Glass	9.7	0.835	32	ε_w	S, SW, Bo, SLo

Table 1.3 Summery of Experimental Systems of Liquid -Liquid Vertical Upflow

Authors	D [cm] pipe material	μ_o/μ_w	ρ_o/ρ_w	σ dyne/cm	Additional Measurements
Govier *et al* (1961)	2.64 Cellulose Acetate-Butyrate	0.936 20.1 150	0.780 0.851 0.880	35.3 50.2 49.8	dp/dl ε_w
Brown & Govier (1961)	2.64 Cellulose Acetate-Butyrate	21.5	0.850	50.34	dp/dl, ε_w Bubble size & velocity
Vigneaux *et al* (1988)	20		0.741		Phase distribution (Impedance probe)
Zavareh *et al* (1988)	18.41 Acrylic	2.46	0.783	52.2	dp/dl ε_w
Hasan & Kabir (1990)	6.35, 12.7 Plexiglass	1.544	0.756		ε_w
Flores (1997)	5.08 Acrylic	20	0.858	33.5	dP/dl ε_w
Hamad *et al* (2000)	7.78 Perspex	1.6	0.803	17	Drop size, velocity & distribution (dual optical probe)
Simmons & Azzopardi (2001)	6.3 PVC	1.125	0.684	10	Drop size, velocity & distribution (Par-Tec 300C, Malvern 2600)

References

Acrivos, A. and Lo, T.S. (1978). Deformation and breakup of a single slender drop in an extensional flow. *Journal Fluid Mechanics* 86:641.

Alkaya, B., Jayawardena, S.S., and Brill J.P. (2000). Oil-water flow patterns in slightly inclined pipes. *In Proceedings 2000 ETCE/OMAE Joint Conference, Petroleum Production Symposium*, New Orleans, 14-17 February, 1-7.

Andreini, P.A., Greeff P., Galbiati, L., Kuklwetter, A. and Sutgia, G. (1997). Oil-water flow in small diameter tubes. *International Symposium on Liquid-Liquid Two-Phase Flow And Transport Phenomena*. Antalya, Turkey, 3-7.

Angeli, P., and Hewitt, G.F. (1996). Pressure-Gradient Phenomenon During Horizontal Oil-Water Flow, *ASME Proceedings OMAE* 5:287-295.

Angeli, P., and Hewitt, G.F. (1998). Pressure gradient in horizontal liquid-liquid flows. *International Journal Multiphase Flow* 24:1183-1203.

Angeli, P., and Hewitt, G.F. (2000). Flow structure in horizontal oil-water flow. *International Journal Multiphase Flow* 26:1117-1140.

Angeli, P., Lovick, S. and Lum, Y.L. (2002). Investigations on the Three-Layer Pattern During L-L Flows, *40th European Two-Phase Flow Group Meeting*, Stockholm, June 10-13.

Arirachakaran, S., Oglesby, K.D., Malinowsky, M.S., Shoham, O., and Brill, J.P. (1989). An Analysis of Oil/Water Flow Phenomena in Horizontal Pipes. *SPE Paper 18836, SPE Professional Product Operating Symposium* , Oklahoma.

Arney, M., Bai, R., Guevara, E., Joseph, D.D. and Liu, K. (1993). Friction factor and holdup studies for lubricated pipelining: I. Experiments and correlations. *International Journal of Multiphase Flow* 19:1061-1076.

Azzopardi, B.J. and Hewitt, G.F. (1997). Maximum drop sizes in gas-liquid flows. *Multiphase Science Technology* 9:109-204.

Bai, R., Chen, K. and Joseph, D.D. (1992). Lubricated pipelining: Stability of core-annular flow, Part V. experiments and comparison with theory, *Journal of Fluid Mechanics* 240:97-132.

Barnea, D. (1987). A Unified model for predicting flow-pattern transitions for the whole range of pipe inclinations. *International Journal Multiphase Flow* 11:1-12.

Baron, T., Sterling, C.S., and Schueler, A.P. (1953). Viscosity of Suspensions - Review and Applications of Two-Phase Flow. *Proceedings 3rd Midwestern Conference Fluid Mechanics*. University of Minnesota, Minneapolis 103-123.

Bentwich, M. (1964). Two-phase axial flow in pipe. *Trans. of the ASME*. Series D 84(4):669-672.

Bentwich, M., Kelly, D.A.I. and Epstein, N. (1970). Two-Phase Eccentric Interface Laminar Pipeline Flow. *J. Basic Engineering* 92:32-36.

Bentwich, M. (1976). Two-phase laminar flow in a pipe with naturally curved interface. *Chemical Engineering Sciences* 31:71-76.

Beretta, A., Ferrari, P., Galbiodi, L., Andreini, P.A. (1997). Oil-Water Flow in Small Diameter Tubes. Pressure Drop. *International Comm. Heat Mass Transfer* 24(2):231-239.

Beretta, A., Ferrari, P., Galbiodi, L., Andreini, P.A. (1997). Oil-Water Flow in Small Diameter Tubes. Flow Patterns. *International Comm. Heat Mass Transfer* 24(2):223-229.

Biberg, D., Halvorsen, G. (2000). Wall and interfacial shear stress in pressure driven two-phase laminar stratified pipe flow. *International Journal Multiphase Flow* 26:1645-1673.

Brauner, N., and Moalem Maron, D. (1989). Two-phase liquid liquid stratified flow, PCH Physico Chemica, *Hydrodynamics* 11(4):487-506.

Brauner, N. (1990). On the Relation Between Two-Phase Flow Under Reduced Gravity and Earth Experiment. *International Comm. Heat Mass Transfer* 17(3):271-282.

Brauner, N., and Moalem Maron, D. (1991). Analysis of stratified/nonstratified transitional boundaries in horizontal gas-liquid flows. *Chemical Engineering Science* 46(7):1849-1859.

Brauner, N. (1991). Two-Phase Liquid-Liquid Annular Flow. *International Journal Multiphase Flow*, 17(1):59-76.

Brauner, N., and Moalem Maron, D. (1992a). Stability analysis of stratified liquid-liquid horizontal flow. *International Journal of Multiphase Flow* 18:103-121.

Brauner, N., and Moalem Maron, D. (1992b). Flow pattern transitions in two phase liquid-liquid horizontal tubes *International Journal of Multiphase Flow* 18:123-140.

Brauner, N., and Moalem Maron, D. (1992c). Identification of the range of small diameter conduits regarding two-phase flow patterns transitions. *International Comm. Heat Mass Transfer* 19:29-39.

Brauner, N., and Moalem Maron, D. (1992d). Analysis of stratified/nonstratified transitional boundaries in inclined gas-liquid flows. *International Journal of Multiphase Flow* 18(4):541-557.

Brauner, N., and Moalem Maron, D. (1993). The role of interfacial shear modelling in predicting the stability of stratified two-phase flow. *Chemical Engineering Science* 8(10):2867-2879.

Brauner, N., and Moalem Maron, D. (1994). Stability of two-phase stratified flow as controlled by laminar turbulent transition. *International Comm. Heat Mass Transfer*, 21:65-74.

Brauner, N., Rovinsky, J. and Moalem Maron, D. (1995a). Analytical Solution of Laminar-Laminar Stratified Two-Phase Flows with Curved Interfaces, *Proceedings of the 7th International Meeting of Nuclear Rector Thermal-Hydraulics* NURETh-7(1):192-211.

Brauner, N. (1996). Role of Interfacial Shear Modelling in Predicting Stability of Stratified Two-Phase Flow, in Encyclopedia of Fluid Mechanics, edited by N.P. Cheremisinoff. Advances in Engineering Fluid Mechanics: Boundary Conditions Required for CFD Simulation, 5:317-378.

Brauner, N., Rovinsky, J., and Moalem Maron, D. (1996a). Analytical solution for laminar-laminar two-phase stratified flow in circular conduits. *Chemical Engineering Comm.* 141-142, 103-143.

Brauner, N., Rovinsky, J. and Moalem Maron, D. (1996b). Determination of the Interface Curvature in Stratified Two-Phase Systems by Energy Considerations. *International Journal Multiphase Flow* 22:1167-1185.

Brauner, N. (1997). Consistent Closure Laws for Modelling Two-Phase Annular Flow Via Two-Fluid Approach. *Internal Report*, Tel-Aviv University, Faculty of Engineering, October.

Brauner, N., Moalem Maron, D. and Rovinsky, J. (1997). Characteristics of Annular and Stratified Two-Phase Flows in the Limit of a Fully Eccentric Core Annular Configuration, *Proc. of the ExHFT-4*, Brussels, 2:1189-1196.

Brauner, N. (1998). Liquid-Liquid Two-Phase Flow, Chap. 2.3.5 in HEDU - Heat Exchanger Design Update, edited by G.F. Hewitt 1:40.

Brauner, N., Moalem Maron, D. and Rovinsky, J. (1998). A Two-Fluid Model for Stratified Flows with Curved Interfaces. *International Journal Multiphase Flow*. 24:975-1004.

Brauner, N. (2000). The onset of drops atomization and the prediction of annular flow boundaries in two-phase pipe flow. Internal Report-5101, Faculty of Engineering, Tel-Aviv, Israel.

Brauner, N. (2001). The Prediction of Dispersed Flows Boundaries in Liquid-Liquid and Gas-Liquid Systems, *International Journal Multiphase Flow* 27(5):911-928

Brauner, N. and Ullmann, A. (2002). Modelling of Phase Inversion Phenomenon in Two-Phase Pipe Flow, *International Journal Multiphase Flow*. In print.

Brodkey, R.S. (1969). *The Phenomena of Fluid Motions*. Addison-Wesley, Reading, MA.

Brown, R.A.S., and Govier, G.W. (1961). High-Speed Photography in the Study of Two-Phase Flow. *Canadian Journal Chemical Engineering* 159-164.

Chesters, A.K. (1991). The Modelling of Coalescence Process in Fluid-Liquid Dispersions. *Chemical Engineering Res. Des., Part A* 69(A4):259-270.

Cohen, R.D. (1991). Shattering of Liquid Drop due to Impact. *Proceedings Royal Society, London* A435:483-503.

Charles, M.E., Govier, G.W., and Hodgson, G.W. (1961). The horizontal flow of equal density oil-water mixtures, *Canadian Journal of Chemical Engineering*, 39:287-36.

Charles, M.E., and Lilleleht, L.U. (1966). Correlation of Pressure Gradients for the Stratified Laminar-Turbulent Pipeline Flow of Two Immiscible Liquids. *Canadian Journal Chemical Engineering* 44:47-49.

Clift, R., Grace, J.R., and Weber, M.E. (1978). Bubbles, Drops and Particles. Academic Press.

Colebrook, C. (1938-39). Turbulent Flow in Pipes with Particular Reference to the Transition Region Between the Smooth and Rough Pipe Laws. *Journal Inst. Cir. Engineering* 11:133-156.

Cox, A.L. (1986). A Study of Horizontal and Downhill Two-Phase Oil-Water Flow, M.S. Thesis, The University of Texas.

Davies, J.T. (1987). A physical interpretation of drop sizes in homogenizers agitated viscous oils. *Chemical Engineering Science* 42(7):1671-1676.

Decarre, S., and Fabre, J. (1997). Phase inversion behavior for liquid-liquid dispersions, *Revue Institution Francais du Petiale*. 52:415-424.

Ding, Z.X., Ullah, K., and Huang, Y. (1994). A comparison of predictive oil/water holdup models for production log interpretation in vertical and deviated wellbores, in In Proceedings SPWLA 35th Annual Logging Symposium, Tulsa, OK, USA, June 19-22, 1-12.

Epstein, N., Bianchi, R.J., Lee, V.T.Y., and Bentwich, M. (1974). Eccentric Laminar Couette Flow of Long Cylindrical Capsules, *Canadian Journal of Chemical Engineering*. 52:210-214.

Fairuzov, Y.V., Medina, P.A., Fierro, J.V. Islas, R.G. (2000). Flow pattern transitions in horizontal pipelines carrying oil-water mixtures: full-scale experiments. *Journal Energy Resources Technology-Trans. ASME* 122:169-176.

Flores, J.G. (1997). *Oil-Water Flow in Vertical and Deviated Wells*. Ph.D. Dissertation, The University of Tulsa, Tulsa, Oklahoma.

Flores, J.G., Chen, X.T., Sarica, C., and Brill, J.P. (1997). Characterization of Oil-Water Flow Patterns in Vertical and Deviated Wells. *1997 SPE Annual Technical Conference and Exhibition*. San Antonio, Texas, SPE paper 38810 1-10.

Fujii, T., Otha, J., Nakazawa, T., and Morimoto, O. (1994). The Behavior of an Immiscible Equal-Density Liquid-Liquid Two-Phase Flow in a Horizontal Tube. *JSME Journal Series B, Fluids and Thermal Engineering*, 30(1):22-29.

Garner, R.G., and Raithby, G.D. (1978). Laminar Flow Between a Circular Tube and a Cylindrical Eccentric Capsule, *Canadian Journal of Chemical Engineering*. 56:176-180.

Gat S., (2002). *Two-Phase Liquid-Liquid Concurrent flow in Inclined Tubes*. M.Sc. Thesis, Faculty of Engineering, Tel-Aviv University.

Goldstein, A. (2000). *Analytical Solution of Two-Phase Laminar Stratified Flow in Inclined Tubes*, M.Sc. Thesis.

Gorelic, D. and Brauner, N. (1999). The Interface Configuration in Two-Phase Stratified Flow, *International Journal Multiphase Flow*. 25:877-1007.

Govier, G.W., Sullivan, G.A., and Wood, R.K. (1961). The Upward Vertical Flow of Oil-Water Mixtures. *Canadian Journal of Chemical Engineering* 9:67-75.

Govier, G.W., and Aziz, K. (1972). The Flow of Complex Mixtures in Pipes, Robert E. Krieger Publishing Company, 1st ed., 326-327, New York.

Grace, J.R., Wairegi, T., and Brophy, J. (1978). Break-up of Drops and Bubbles in Stagnant Media. *Canadian Journal of Chemical Engineering* 56:3-8.

Guevara, E., Zagustin, K., Zubillaga, V., and Trallero, J.L. (1988). Core-Annular Flow (CAF): The Most Economical Method for the Transportation of Viscous Hydrocarbons, 4th UNITAR/U.N. Dev. Program AOSTRA-Petro-Can-Pet. Venez., S.A.-DOE Heavy Crude Tar Sands. *International Conference Edmonton*. 5:194.

Guzhov, A., Grishin, A.D., Medredev, V.F. and Medredeva, O.P. (1973). Emulsion formation during the flow of two immiscible liquids. *Neft. Choz.* (in Russian). 8:58-61.

Hall, A.R., and Hewitt, G.F. (1993). Application of two-fluid analysis to laminar stratified oil-water flows. *International Journal Multiphase Flow*. 19:4 711-717.

Hamad, F.A., Pierscionek, B.K., Brunn, H.H. (2000). A Dual Optical Probe for Volume Fraction, Drop Velocity and Drop Size Measurements in Liquid-Liquid Two-Phase Flow. *Meas. Science Technology* 11:1307-1318.

Hanks, R. and Christianson, E.B. (1962). The Laminar-Turbulent Transition in Normothermia Flow of Pseudoplastic Fluids in Tubes. *AIChE Journal* 8(4):467-471.

Hapanowicz, J., Troniewski, L., and Witczak S. (1997). Flow Patterns of Water-Oil Mixture Flowing in Horizontal Pipes, *International Symposium on Liquid-Liquid Two-Phase Flow and Transport Phenomena*, Antalya, Turkey, 3-7 Nov.

Harmathy, T.Z. (1960). Velocity of Large Drops and Bubbles in Media of Infinite or Restricted Extent. *AIChE Journal* 6(2):281-288.

Hasan, A.R., and Kabir, C.S. (1990). A New Model for Two-Phase Oil/Water Flow; Production Log Interpretation and Tubular Calculations. *SPE Production Engineering*, 193-199.

Hasan, A.R. and Kabir, C.S. (1999). A simplified model for oil/water flow in vertical and deviated wellbores, *SPE In Proceedings and Facilities*, 141:56-62.

Hasson, D., Mann, U., and Nir A. (1970). Annular Flow of Two Immiscible Liquids: I, Mechanisms, *Canadian Journal of Chemical Engineering*. 48:514-520.

Hasson, D. and Nir, A (1970). Annular Flow of Two Immiscible Liquids: II, *Canadian Journal of Chemical Engineering*. 48:521-526.

Hasson, D. (1978). Scale Prevention by Annular Flow of an Immiscible Liquid Along the Walls of a Heated Tube, *Proc. 6th International Heat Toronto*. 4:391-397.

Hill, A.D., and Oolman, T. (1982). Production Logging Tool Behavior in Two-Phase Inclined Flow. *JPT* 2432-2440.

Hinze, J. (1955). Fundamentals of the Hydrodynamic Mechanism of Splitting in Dispersion Process. *AIChE Journal* 1(3):289-295.

Hinze, J.O. (1959). *Turbulence*. McGraw-Hill, New York.

Ho, W.S., and Li,N.N. (1994). Core Annular Flow of Liquid Membrane Emulsion, *AIChE Journal*, 40:1961-1968.

Huang, A., Christodoulou, C., and Joseph, D.D. (1994). Friction Factor and Holdup Studies for Lubricated Pipelining. *International Journal Multiphase Flow* 20:481-494.

Hughmark, G.A. (1971). Drop Breakup in Turbulent Pipe Flow. *AIChE Journal* 4:1000.

Joseph, D.D., and Renardy, Y.Y. (1992). Fundamentals of Two Fluids Dynamics Part I and II (edited by F. John, et al), Springer-Verlag.

Kitscha, J. and Kocamustafaogullari, G. (1989). Breakup Criteria for Fluid Particles. *International Journal Multiphase Flow* 15:573:588.

Kolmogorov, A.N. (1949). On the Breaking of Drops in Turbulent Flow. *Doklady Akad. Nauk.* 66:825-828.

Kruyer, J., Redberger, P.J., and Ellis, H.S. (1967). The Pipeline Flow of Capsules - Part 9, *Journal Fluid Mechanics*. 30:513-531.

Kubie, J. and Gardner, G.C. (1977). Drop Sizes and Drop Dispersion in Straight Horizontal Tubes and in Helical Coils. *Chemical Engineering Science* 32:195-202.

Kurban, A.P.A. (1997). *Stratified Liquid-Liquid Flow*. Ph.D. Dissertation, Imperial College, London, U.K.

Laflin, G.C., and Oglesby, K.D. (1976). An Experimental Study on the Effect of Flow Rate, Water Fraction, and Gas-Liquid Ratio on Air-Oil-Water Flow in Horizontal Pipes. B.S. Thesis, University of Tulsa.

Luhning, R.W. and Sawistowki, H. (1971). Phase inversion in stirred liquid-liquid systems. *Proceedings International Solvent Extr. Conference*, The Hague, Society of Chemical Industry, London. 883-887.

Malinowsky, M.S. (1975). An Experimental Study of Oil-Water and Air-Oil-Water Flowing Mixtures in Horizontal Pipes, M.S. Thesis, University of Tulsa.

Masliyah, H. & Shook C.A. (1978). Two-phase laminar zero net flow in circular inclined pipe. *The Canadian Journal Chemical Engineering*, 56:165-175.

McAulifee, C.D. (1973). Oil-in-Water Emulsions and Their Flow Properties in Porous Meida. *Journal Petroleum Technology* 727-733.

Miesen, R., Beijnon, G., Duijvestijn, P.E.M., Oliemans, R.V.A., and Verheggen, T. (1992). Interfacial Waves in Core-Annular Flow, *Journal Fluid Mechanics*, 238(97).

Moalem-Maron, D., Brauner, N., and Rovinsky, J. (1995). Analytical Prediction of the Interface Curvature and its Effects on the Stratified Two-Phase Characteristics. *Proceedings of the International Symposium Two-Phase Flow Modelling and Experimentation* 1:163-170.

Mukherjee, H.K., Brill, J.P. and Beggs H.D. (1981). Experimental Study of Oil-Water Flow in Inclined Pipes, *Transactions of the ASME*, 103:56-66.

Mukhopadhyay, H. (1977). An Experimental Study of Two-Phase Oil-Water Flow in Inclined Pipes, M.S. Thesis, U. of Tulsa.

Nadler, M. Mewes, D. (1997). Flow induced emulsification in the flow of two immiscible liquids in horizontal pipes. *International Journal Multiphase Flow* 23(1):55-68.

Ng, T.S., Lawrence, C.J., Hewitt, G.F. (2001). Interface shapes for two-phase laminar stratified flow in a circular pipe. *International Journal Multiphase Flow* 27:1301-1311.

Ng, T.S., Lawrence, C.J., Hewitt, G.F. (2002). Laminar stratified pipe flow. *International Journal Multiphase Flow* 28(6):963-996.

Oglesby, K.D. (1979). An Experimental Study on the Effects of Oil Viscosity Mixture Velocity, and Water Fraction on Horizontal Oil-Water Flow, M.S. Thesis, University of Tulsa.

Oliemans, R.V.A. (1986). *The Lubricating Film Model for Core-Annular Flow*. Ph.D. Dissertation, Delft University Press.

Oliemans, R.V.A., Ooms, G. (1986). Core-Annular Flow of Oil and Water Through a Pipeline. *Multiphase Science and Technology*. vol. 2, eds. G.F. Hewitt, J.M. Delhaye, and N. Zuber, Hemisphere Publishing Corporation, Washington.

Ong, J., Enden, G. & Popel A.S. (1994). Converging three dimensional Stokes flow of two fluids in a T-type bifurcation, *Journal Fluid Mechanics* 270:51-71.

Ooms, G., Segal, A., Van der Wees, A.J., Meerhoff, R., and Oliemans, R.V.A. (1984). Theoretical Model for Core-Annular Flow of a Very Viscous Oil Core and a Water Annulus Through a Horizontal Pipe. *International Journal Multiphase Flow*, 10:41-60.

Ooms, G., Segal, A., Cheung, S.Y., and Oliemans, R.V.A. (1985). Propagation of Long Waves of Finite Amplitude at the Interface of Two Viscous Fluids. *International Journal Multiphase Flow* 10:481-502.

Pal, R. (1990). On the Flow Characteristics of Highly Concentrated Oil-in-Water Emulsions. *The Chemical Engineering Journal* 43:53-57.

Pan, L., Jayanti, S., and Hewitt, G.F. (1995). Flow Patterns, phase inversion and pressure gradients in air oil water flow in horizontal pipe, *Proceedings of the ICMF'95*, Kyoto, Japan, paper FT2.

Paul, H.I. and Sleicher Jr., C.A. (1965). The Maximum Stable Drop Size in Turbulent Flow: Effect of Pipe Diameter. *Chemical Engineering Science* 20:57-59.

Pilehvari, A., Saadevandi, B., Halvaci, M. and Clark, P.E. (1988). Oil/Water Emulsions for Pipeline Transport of Viscous Crude Oil. *Paper SPE 18218, SPE. Annual Technology Conference & Exhibition* Houston.

Ranger, K.B. & Davis A.M.J. (1979). Steady pressure driven two-phase stratified laminar flow through a pipe. *Canadian Journal of Chemical Engineering* 57:688-691.

Rovinsky, J., Brauner, N. and Moalem Maron, D. (1997). Analytical Solution for Laminar Two-Phase Flow in a Fully Eccentric Core-Annular Configuration, *International Journal Multiphase Flow* 23:523-542.

Russell, T.W.F. and Charles, M.E. (1959). The Effect of the Less Viscous Liquid in the Laminar Flow of Two Immiscible Liquids. *Canadian Journal Chemical Engineering* 37:18-34.

Russell, T.W.F., Hodgson, G.W., and Govier, G.W. (1959). Horizontal pipeline flow of oil and water, Can. Journal of Chemical Engineering, 37: 9-17.

Semenov, N.L. & Tochigin, A.A. (1962). An analytical study of the separate laminar flow of a two-phase mixture in inclined pipes. *Journal Engineering Physics* 4:29.

Shacham, M., and Brauner, N. (2002). Numerical solution of non-linear algebraic equations with discontinuities. Comp. and Chemical Engineering. in print.

Schramm, L.L. (1992). Emulsions Fundamentals and Applications in the Petroleum Industry. *Advances in Applications in the Petroleum Industry, Advances in Chemistry Series 231, American Chemical Society.*

Scot, P.M. and Knudsen, J.G. (1972). Two-Phase Liquid-Liquid Flow in Pipes. *AIChE Symposium Series* 68(118):38-44.

Scott, G.M. (1985). A Study of Two-Phase Liquid-Liquid Flow at Variable Inclinations, M.S. Thesis, The University of Texas.

Sherman, P. (1968). *Emulsion Science*, (editor), Academic Press, New York.

Simmons, M.J.H. (2001). Drop size Distribution in Dispersed Liquid-Liquid Pipe Flow. *International Journal Multiphase Flow* 23:843-859.

Sinclair, A.R. (1970). Rheology of Viscous Fracturing Fluids. *Journal Petroleum Technology* 711-719.

Soleimani, A. (1999) . *Phase distribution and associated phenomena in oil-water flows in horizontal tubes*. Ph.D. Dissertation. Imperial College, University of London.

Stalpelberg, H.H., and Mewes, D. (1990). The flow of two immiscible liquids and air in horizontal gas-liquid pipe, Winter Annual Meeting of the ASME, 89-96.

Tabeling, P., Pouliquen, O., Theron, B., and Catala G. (1991). Oil water flows in deviated pipes: experimental study and modelling. *In Proceedings of the 5th International Conference on Multiphase Flow Production*, Cannes, France, June 19-21, 294-306.

Tang, Y.P., Himmelblau, D.M. (1963). Velocity Distribution of Isothermal Two-Phase Cocurrent Laminar Flow in Horizontal Rectangular Duct. *Chemical Engineering Science*. 18:143-144.

Taylor, G.I. (1934). The Formation of Emulsions in Definable Fields of Flow, *Proceedings Royal Society London A* 146:501-523.

Theissing, P.A. (1980). A Generally Valid Method for Calculating Frictional Pressure Drop in Multiphase Flow. *Chemical Ing. Technik*. 52:344-355. (In German).

Tidhar, M., Merchuk, J.C., Sembira, A.N., Wolf, D. (1986). Characteristics of a motionless mixer for dispersion of immiscible fluids – II. Phase inversion of liquid-liquid systems. *Chemical Engineering Science*, 41(3):457-462.

Trallero, J.L. (1995). *Oil-Water Flow Patterns in Horizontal Pipes*. Ph.D. Dissertation, The University of Tulsa.

Tsouris, C. and Tavlarides, L.L. (1994). Breakage and Coalescence Models for Drops in Turbulent Dispersions. *AIChE Journal* 40(3):395-406.

Ullmann, A., Zamir, M. Ludmer, Z., Brauner, N. (2000). Characteristics of Liquid-Liquid Counetr-Current Flow in Inclined Tubes - Application to PTE Process, Proc. of the International Symp on Multiphase Flow and Transport Phenomenon, Antalya, Turkey, Nov. 5-10. ICHMT 112-116.

Ullmann, A., Zamir, M., Ludmer L. and Brauner, N. (2001a). Flow Patterns and Flooding Mechanisms in Liquid-Liquid Counter-current Flow in Inclined Tubes, ICMF-2001, New Orleans, Louisiana, May 27-June 1.

Ullmann, A., Zamir, M., Gat S., and Brauner, N. (2001b). Multi-Value Holdups in Stratified Co-current and Counter-current Inclined Two-Phase Flows, 39th European Two-Phase Flow Group Meeting, Aveiro, Portugal, 17-20.

Ullman, A., Zamir, M., Ludmer, Z., and Brauner, N. (2002a). Counter-current Flow of Two Liquid Phases in an Inclined Tube: Part I. Submitted.

Ullman, A., Zamir, M., Gat, S., and Brauner, N. (2002b). Counter-current Flow of Two Liquid Phases in an Inclined Tube: Part II. Submitted.

Valle, A., and Kvandal, H.K. (1995). Pressure drop and dispersion characteristics of separated oil-water flow. In Celata, G.P., and Shah, R.K. Edizioni ETS, eds., In Proceedings of the International Symposium on Two-Phase Flow Modelling and Experimentation, Oct. 9-11, Rome, Italy, 583-591.

Valle, A., and Utvik, O.H.(1997). Pressure drop, flow pattern and slip for two phase crude oil/water flow: experiments and model predictions, International Symposium on Liquid-Liquid Two-Phase Flow and Transport Phenomena, Antalya, Turkey, 3-7 Nov.

Vedapuri, D., Bessette, D. and Jepson, W.P. (1997). A segregated flow model to predict water layer thickness in oil-water flows in horizontal and slightly inclined pipelines, in In Proceedings Multiphase'97, Cannes, France June 18-20, 75-105.

Vigneaux, P., Chenois, P. and Hulin, J.P. (1988). Liquid-Liquid Flows in an Inclined Pipe. *AIChE Journal* 34:781-789.

Wu, H.L., Duijrestijn, P.E.M. (1986). Core-Annular Flow: A Solution to Pipeline Transportation of Heavy Crude Oils. *Review Tec. INTERVER*, 6(1):17-22.

Yeh, G. Haynie Jr., F.H., Moses, R.E. (1964). Phase-Volume Relationship at the Point of Phase Inversion in Liquid Dispersion. *AIChE Journal.* 10(2):260-265.

Yeo, L.Y., Mater, O.K., Perez de Ortiz, E.S., Hewitt, G.F. (2000). Phase inversion and associated phenomena. *Multiphase Science & Technology*, 12:51-116.

Zamir, M. (1998). *Multistage Extraction in an Inclined Column Based on a Phase Transition of Critical-Solution Mixtures*. Ph.D. Dissertation.

Zavareh, F., Hill, A.D. and Podio, A.L. (1988). Flow Regimes in Vertical and Inclined Oil/Water Flow in Pipes, Paper SPE 18215, Presented at the 63rd Annual Technical Conference and Exhibition, Houston, Texas, Oct. 2-5.

Zigrang D.I. and Sylvester, N.D. (1985). A Review of Explicit Friction Factor Equations. *Journal Energy Res. Technology* 107:280-283.

Zuber, N. and Findlay, I. (1965). *Trans. J. Heat Transfer*. ASME 87:453-468.

Zukoski, E.E. (1966). Influence of Viscosity, Surface Tension and Inclination Angle on Motion of Long Bubbles in Closed Tubes. *Journal Fluid Mechanics* 25:821-837.